

1 **Molecular and seasonal characteristics of organic vapors in**
2 **urban Beijing: insights from Vocus-PTR measurements**

3

4 Zhaojin An^{1,2}, Rujing Yin³, Xinyan Zhao¹, Xiaoxiao Li⁴, Yuyang Li¹, Yi Yuan¹,
5 Junchen Guo¹, Yiqi Zhao¹, Xue Li⁵, Dandan Li¹, Yaowei Li², Dongbin Wang¹,
6 Chao Yan⁶, Kebin He¹, Douglas R. Worsnop^{7,8}, Frank N. Keutsch², Jingkun
7 Jiang^{1,*}

8

9 ¹State Key Joint Laboratory of Environment Simulation and Pollution Control,
10 School of Environment, Tsinghua University, 100084, Beijing, China

11 ²School of Engineering and Applied Sciences, Harvard University, Cambridge,
12 Massachusetts 02138, USA

13 ³Key Laboratory of Industrial Ecology and Environmental Engineering (Ministry
14 of Education), School of Environmental Science and Technology, Dalian
15 University of Technology, 116024, Dalian, China

16 ⁴School of Resource and Environmental Sciences, Wuhan University, 430072,
17 Wuhan, China

18 ⁵School of Environment, Henan Normal University, 453007, Xinxiang, China

19 ⁶Joint International Research Laboratory of Atmospheric and Earth System
20 Research, School of Atmospheric Sciences, Nanjing University, 210023,
21 Nanjing, China

22 ⁷Institute for Atmospheric and earth System Research / Physics, Faculty of
23 Science, University of Helsinki, Helsinki 00014, Finland

24 ⁸Aerodyne Research, Inc., Billerica, Massachusetts 01821, USA

25 *Corresponding author: Jingkun Jiang (email: jiangjk@tsinghua.edu.cn)

26

27

28 Abstract

29 Understanding the composition and evolution of atmospheric organic vapors is
30 crucial for exploring their impact on air quality. However, the molecular and
31 seasonal characteristics of organic vapors in urban areas, with complex
32 anthropogenic emissions and high variability, remain inadequately understood.
33 In this study, we conducted measurements in urban Beijing during 2021-2022
34 covering four seasons using an improved Proton Transfer Reaction-Mass
35 Spectrometry (Vocus-PTR MS). During the measurement period, a total of
36 895 peaks were observed, and 512 of them can be assigned to formulas. The
37 contribution of $C_xH_yO_z$ species is most significant, which composes up to 54%
38 of the number and 74% of the mixing ratio of total organics. With enhanced
39 sensitivity and mass resolution, various species with sub-ppt level or multiple
40 oxygens (≥ 3) were observed, with 44% of the number measured at sub-ppt
41 level and ~~34~~³⁸% of the number containing 3-8 oxygens. Organic vapors with
42 multiple oxygens mainly consist of intermediate/semi-volatile compounds, and
43 many ~~of~~ formulae detected were reported to be the oxidation products of
44 various volatile organic precursors. In summer, the fast photooxidation process
45 generated organic vapors with multiple oxygens and lead to an increase in both
46 their mixing ratio and proportion. While in other seasons, the variations of
47 organic vapors with multiple oxygens ~~are~~were closely correlated with those of
48 organic vapors with 1-2 oxygens, which could be substantially influenced by
49 primary emissions. Organic vapors with low oxygen content (≤ 2 oxygens) are
50 comparable to the results obtained by traditional PTR-MS measurements in
51 both urban Beijing and neighboring regions.
52

53 1 Introduction

54 Volatile organic compounds (VOCs) play a crucial role in the formation of ozone
55 and fine particulate matter (PM_{2.5}) in the atmosphere, subsequently affecting air
56 quality, climate, and human health (Carter, 1994; Williams and Kopppmann,
57 2007; Jimenez et al., 2009; Hallquist et al., 2009). The sources and atmospheric
58 evolution of VOCs in the atmosphere are complex due to the coexistence of
59 compounds from primary emissions as well as secondary formation (Gentner
60 et al., 2013; Gilman et al., 2015; Millet et al., 2015). Understanding their
61 molecular characteristics is essential for studying their hydroxyl radical (OH)
62 reactivities, ozone and secondary organic aerosol (SOA) formation potentials.
63 However, the diverse range of species and wide distribution of oxidation
64 products of atmospheric VOCs make it challenging to unravel their molecular
65 properties (Goldstein and Galbally, 2007).

66 Instrumental advances have allowed for improving the understanding of the
67 compositions and variations of VOCs at the molecular level, especially for
68 oxygenated VOCs (OVOCs). Gas chromatography or multidimensional gas
69 chromatography coupled with mass spectrometry is the most commonly used
70 technology for VOC measurement, capable of detecting major non-methane
71 hydrocarbons and select OVOCs (Lewis et al., 2000; Xu et al., 2003; Noziere
72 et al., 2015). Proton Transfer Reaction-Mass Spectrometry (PTR-MS) enables
73 real-time detection of VOCs without pre-concentration and separation, greatly
74 enriching the molecular understanding of OVOCs due to its high sensitivity to
75 oxygen-containing compounds (Hansel et al., 1995; De Gouw and Warneke,
76 2007; Yuan et al., 2017). Hundreds of OVOCs ~~are~~ have been detected and
77 characterized in different areas using PTR-MS, e.g. urban (Wu et al., 2020),
78 suburban (He et al., 2022), and forest areas (Pugliese et al., 2023). Recent
79 developments in the ion-molecule reactor (IMR) configuration have greatly
80 increased sensitivities and concurrently lowered the limits of detection of PTR-
81 MS by several orders of magnitude by incorporating radio frequency electric
82 fields to focus ions (Breitenlechner et al., 2017; Krechmer et al., 2018; Reinecke
83 et al., 2023). A consequential issue is that these advanced PTR-MS typically
84 need to eliminate lighter ions to protect the detector from overload, and similar
85 to traditional PTR-MS, they are incapable of obtaining molecular structure
86 information.

87 These improvements have expanded the detection capabilities of PTR-MS,
88 particularly for organic vapors with lower volatility and multiple oxygens (≥ 3)
89 (Riva et al., 2019), which enables the simultaneous measurement of VOC
90 precursors and their primary, secondary, and higher-level oxidation products
91 using a single instrument (Li et al., 2020). Despite their low concentrations,
92 these vapors may condense on pre-existing aerosols and make a significant
93 contribution to secondary aerosol growth and cloud condensation nuclei

94 (Bianchi et al., 2019; Pospisilova et al., 2020; Nie et al., 2022). Organic vapors
95 with multiple oxygens are likely to be simultaneously detected by other chemical
96 ionization mass spectrometry (CIMS), e.g., nitrate (NO_3^-), iodide (I^-), bromide
97 (Br^-), and ammonium (NH_4^+) (Riva et al., 2019; Huang et al., 2021), which are
98 widely used for measuring oxygenated organic compounds in the atmosphere
99 (Bianchi et al., 2019; Ye et al., 2021; Huang et al., 2021). Therefore, using these
100 improved PTR-MS can supplement our understanding of oxygenated organic
101 vapors and facilitate the study of atmospheric chemical evolution of organics
102 (Wang et al., 2020a).

103 The improved PTR-MS systems have gradually gained traction in research
104 applications over the past few years, including measuring organics in controlled
105 lab studies (Zaytsev et al., 2019a; Zaytsev et al., 2019b; Riva et al., 2019; Li et
106 al., 2022a; Li et al., 2024a), emission sources (Sreeram et al., 2022; Yu et al.,
107 2022; Yacovitch et al., 2023; Wohl et al., 2023; Jahn et al., 2023), and ambient
108 air. For ambient measurements, observations in forested regions have been
109 extensively conducted to study the compositions, variations, fluxes, and
110 emissions of organics from different plants (Li et al., 2020; Li et al., 2021; Huang
111 et al., 2021; Fischer et al., 2021; Thomas et al., 2022; Vettikkat et al., 2023;
112 Vermeuel et al., 2023). Terpenes and their oxidation products with oxygen
113 number up to 6 have been detected (Li et al., 2020). Diterpenes have been
114 directly observed in the ambient air for the first time owing to the substantial
115 improvement in sensitivity of Vocus-PTR (Li et al., 2020). Ambient
116 measurement has been also conducted on a mountain in China, which found
117 that terpenes and their oxidation products dominate the detected organic
118 compounds, while the influence of industrial emissions can also be observed
119 (Zhang et al., 2024).

120 In urban atmospheres, the sources and evolution of VOCs are considerably
121 complex, potentially exhibiting distinct characteristics compared to forested
122 areas. Several studies have carried out measurements in urban air using these
123 improved PTR-MS. Jensen et al. (2023) conducted a one-month observation to
124 address the production of reliable measurements. Coggon et al. (2024)
125 evaluated the fragmentation and interferences of a series of urban VOCs.
126 Pfannerstill et al. (2023 and 2024) measured hundreds of VOCs to calculate
127 their emission fluxes in Los Angeles. A few low-signal species including
128 dimethylamine, icosanal, dimethyl disulfide, and siloxanes emitted from diverse
129 emission sources have been detected as a result of the enhanced sensitivity
130 (Wang et al., 2020b; Chang et al., 2022; Jensen et al., 2023). However, the
131 understanding of organic vapors with multiple oxygens in urban air, including
132 their species, mixing ratios, diurnal profiles, and seasonal variations, remains
133 inadequate.

134 In this study, we conducted measurements of organic vapors using a Vocus-
135 PTR in urban Beijing during 2021-2022, covering four seasons. We present

136 general characteristics of measured organic vapors and compare them with
137 traditional PTR-MS and previous Vocus-PTR measurements. We focus on
138 organic vapors with multiple oxygens (three or more), which have rarely been
139 individually analyzed in previous studies due to their low mixing ratios. Their
140 chemical compositions, atmospheric mixing ratios, diurnal and seasonal
141 variations are reported. Cluster analysis is further conducted to resolve the
142 main driving factors of their variations.

143 **2 Methods**

144 **2.1 Measurements**

145 The observation site is located in the central area of Tsinghua University, Beijing
146 (40°0'N, 116°20'E). It is an urban site with no significant direct influence from
147 industrial activities or heavy-traffic arteries ([Fig. S1](#) in the supporting information,
148 SI). Details of this site can be found in the previous study (Cai and Jiang, 2017).
149 Organic vapors were measured by a Vocus-2R PTR-TOF-MS (Tofwerk AG and
150 Aerodyne Research Inc., referred to as Vocus-PTR hereinafter), which is
151 situated on top of a fourth-floor tower building, with its sampling inlet positioned
152 approximately 20 meters above the ground. The observation period is from May
153 1st, 2021 to March 10th, 2022, covering four seasons. Detailed information about
154 observation periods and their corresponding seasons is shown in [Table S1](#).

155 The operating parameters of the Vocus-PTR used in this study are briefly
156 described here. In PTR-MS, VOCs are ionized via proton transfer by hydronium
157 ions (H_3O^+) in the IMR (Hansel et al., 1995; Yuan et al., 2016). The sensitivity
158 can be quantified based on the proton transfer reaction rate while
159 simultaneously considering ion transmission, detector efficiency, etc. (Cappellin
160 et al., 2012; Jensen et al., 2023). The ion source was supplied with a water
161 vapor flow of 20 sccm. The IMR was operated at 100°C and 2 mbar with axial
162 voltage of 600 V and quadrupole amplitude voltage of 450 V. The IMR operating
163 parameters were optimized to minimize the formation of water clusters. Mass
164 spectra were collected from m/z 11 to m/z 398 with a time resolution of 5 s,
165 achieving a mass resolution $\sim 10,000$ for C_7H_9^+ throughout the measurement
166 period. Ambient air was sampled via a tetrafluoroethylene (PTFE) tube (1.35 m
167 long, 1/4-inch OD) at a flow rate of 3 LPM to reduce wall losses, with only 150
168 sccm flow entering the Vocus-PTR. The sampling tube was heated to $50 \pm 5^\circ\text{C}$
169 during the measurement. A regularly replaced Teflon filter (every 7 days) was
170 used in front of the sampling line to prevent the orifice from clogging. The data
171 within 30 minutes after membrane replacement was excluded. Measurements
172 were made on a 2-hour cycle with 110 min for ambient air, 5 min for zero gas,
173 and 5 min for fast calibration. The fast calibrations involved the use of mixed
174 calibration gases, with detailed information available in [Table S2](#).

175 The ambient PM_{2.5}, NO₂, and O₃ data are from a state-operated air quality
176 station (Wanliu station), located approximately 3.6 km away from our
177 observation site. The meteorological parameters, including temperature (T),
178 relative humidity (RH), wind speed, and wind direction are also from Wanliu
179 station. The diurnal variations of PM_{2.5}, O₃, NO_x, RH, and T in four seasons are
180 shown in [Figure S2](#).

181 **2.2 Data processing**

182 Data analysis of Vocus-PTR mass spectra, including mass calibration, baseline
183 subtraction, and high-resolution peak fitting was conducted using Tofware
184 (v3.2.3, Tofwerk AG and Aerodyne Research Inc.) within the Igor Pro 8 platform
185 (WaveMetrics, OR, USA). The ambient mass spectra were averaged over 1 min
186 for subsequent processing in Tofware. The peaklist used for high-resolution
187 peak fitting was manually made based on mass spectra of both clean days
188 (PM_{2.5} < 75 µg/m³) and polluted days (PM_{2.5} ≥ 75 µg/m³). The maximum mass
189 error allowed for identifying peaks is 5-10 ppm, which is consistent of the error
190 of mass calibration. When there are multiple options of formulas meeting the
191 error limit under, especially at high molecular weights, a peak with oxygen
192 numbers ≤ 8 and carbon numbers ≤ 20, and lower degree of unsaturation were
193 selected; otherwise, the peak would be classified as unknown peak. The
194 maximum peak area residual for each unit mass resolution is 5%. Subsequent
195 analysis was performed in MATLAB R2022a (The MathWorks Inc., USA).

196 In PTR-MS, the sensitivities of organic vapors are typically determined through
197 their direct linear correlation with their PTR rate constant (k_{PTR}). Vocus-PTR
198 utilizes a big segmented quadrupole with a high-pass band filter, which detects
199 ions < 35 m/z with reduced transmission efficiency (Krechmer et al., 2018).
200 Consequently, determining sensitivities in Vocus-PTR involves consideration of
201 both reaction efficiency and transmission efficiency. [Figure S3a](#) shows the
202 measured sensitivities of mixed calibration gases and their corresponding k_{PTR}
203 values. The linear regression between k_{PTR} and sensitivities was obtained
204 based on sensitivities of C₇H₉⁺, C₈H₁₁⁺, C₉H₁₃⁺, C₁₀H₉⁺, and C₅H₉O₂⁺ with an R²
205 of 0.87. Sensitivities of other ions in mixed calibration gases may be influenced
206 by transmission (ions labeled as gray) and fragmentation (C₅H₉⁺, C₁₀H₁₇⁺ and
207 C₁₁H₁₁⁺). The transmission efficiency of mixed calibration gases was calculated
208 using sensitivities of mixed calibration gases, as shown in [Figure S3b](#). The
209 transmission efficiency of mixed calibration gases aligns well with the fitted
210 transmission efficiency curve, except for C₅H₉⁺, C₁₀H₁₇⁺ and C₁₁H₁₁⁺, which
211 potentially experience fragmentation (fragmentation of measured ions are
212 discussed below). For organic vapors without standards, their theoretical k_{PTR}
213 were used to constrain sensitivities, while for organic vapors with no theoretical
214 k_{PTR} , an average k_{PTR} of known species, $2.5 \times 10^{-9} \text{ cm}^3 \text{ molecule}^{-1} \text{ s}^{-1}$ was used
215 to constrain their sensitivities. The theoretical k_{PTR} of organic vapors are from

216 previous studies (Zhao and Zhang, 2004; Cappellin et al., 2012; Sekimoto et
217 al., 2017). Average limits of detection (LODs, 1 min) of the measured
218 compounds were determined using zero-gas background measurements taken
219 every 2 hours during the observation periods, as shown in Figure S4. The LODs
220 were calculated as 3 times the standard deviation of the zero-gas background
221 divided by the obtained sensitivity. The LODs show a correlation with masses;
222 as masses increase, instrument backgrounds decrease, leading to lower LODs.
223 This trend was observed for species with different oxygen content, with LODs
224 around 0.03 ± 0.03 pptv at m/z 200. Note that LODs in this study are one-minute
225 averages, with raw 1-second data averaged to 1 minute before ToFware
226 analysis as mentioned before, which may account for the lower LODs
227 compared to those in Jensen et al. (2023). ~~Data below the LODs were excluded
228 from further analysis.~~

229 The fragmentation, water cluster, and interferences for calibrated and
230 uncalibrated species were corrected. The ratio of the electric field strength (E)
231 to the buffer gas number density (N) used in our study was 146.9 Td, and the
232 gradient between BSQ skimmer 1 and skimmer 2 was 9.8 V, which in case
233 limited the formation of water clusters, promoted the simple reaction kinetics,
234 and improved the sensitivity, but may lead to stronger fragmentation. For α -
235 pinene, we identified its fragments based on GC chromatograms. The Vocus-
236 PTR was calibrated in GC mode before atmospheric measurement. A total of 4
237 species were tested in GC mode, including severely fragmented α -pinene. The
238 spectrum of α -pinene showed that the main fragment was $C_6H_9^+$. Several long-
239 chain aldehydes and cycloalkanes may fragment on $C_5H_8H^+$, the ion typically
240 attributed to isoprene in PTR-MS (Gueneron et al., 2015; Pfannerstill et al.,
241 2023a; Coggon et al., 2024). We corrected isoprene signals following an
242 approach by Coggon et al. (2024). The correction was calculated as follows:

$$243 \quad m/z \ 69.07_{\text{Corrected}} = S_{69.07} - S_{111.12+125.13} \cdot f_{69.07/(111.12+125.13)} \quad (1)$$

244 $S_{69.07}$ is the signal measured at $C_5H_9^+$. $S_{111.12+125.13}$ is the signal of the isoprene
245 interferences, referring to $C_8H_{15}^+$ (m/z 111.12) and $C_9H_{17}^+$ (m/z 125.13), which
246 are dehydrated products from octanal and nonanal, respectively.
247 $f_{69.07/(111.12+125.13)}$ was determined from nighttime data (0:00-4:00) of each period.
248 Similarly, acetaldehyde was corrected for ethanol fragments. We also checked
249 the fragments and water cluster list in Pfannerstill et al. (2023a) and Jensen et
250 al. (2023). When the Pearson correlation coefficient r is greater than 0.95, the
251 ions were considered as fragments or water clusters of the parent ion. We also
252 tried to exclude the effects of unknown fragments and water clusters based on
253 correlations of times series. Similar to Pfannerstill et al. (2023a), any ion
254 showing a correlation with another ion with $r^2 > 0.97$ (if chemical reasonable)
255 was analyzed for possible water clustering or fragmentation effects and added
256 up with its parent ion. The ions corrected are ~~specified in Table S3, listed as
257 follows: $C_2H_4N^+$ with water cluster $C_2H_6NO^+$; $C_3H_7O^+$ with water cluster $C_3H_9O_2^+$;~~

~~C₅H₉⁺ with fragment C₅H₇⁺, C₇H₉⁺ with fragment C₇H₇⁺, CH₄NO⁺ with water cluster CH₆NO₂⁺, C₂H₇O⁺ with water cluster C₂H₉O₂⁺, C₃H₃O₂⁺ with water cluster C₃H₅O₃⁺, C₄H₅O₂⁺ with water cluster C₄H₇O₃⁺, C₃H₅⁺ with fragment C₃H₃⁺, C₂H₅O⁺ with water cluster C₂H₇O₂⁺, C₂H₄NO⁺ with water cluster C₂H₆NO₂⁺, C₄H₅O₂⁺ with water cluster C₄H₇O₃⁺, C₃H₃O₃⁺ with water cluster C₃H₅O₄⁺, C₆H₆NO⁺ with water cluster C₆H₈NO₂⁺, C₈H₈NO₂⁺ with water cluster C₈H₁₀NO₃⁺, C₁₀H₂₄O⁺ with water cluster C₁₀H₂₃O₂⁺, C₉H₁₃O₃⁺ with water cluster C₉H₁₅O₄⁺, C₁₀H₁₃O₃⁺ with water cluster C₁₀H₁₅O₄⁺, and C₁₄H₁₃⁺ with water cluster C₁₄H₁₅O⁺.~~

Here, we discuss the uncertainties of quantification for calibrated and uncalibrated compounds. The uncertainty of calibrated ions ranges from 2% to 16% determined from the standard deviations of the fast calibrations during the measurement periods. The **semi**-quantification was conducted for uncalibrated compounds with their sensitivities constrained by k_{PTR} linear relationship and transmission efficiency. The uncertainty of these uncalibrated compounds arising from linear fitting and transmission efficiency fitting is 20% using Monte Carlo simulation. Additionally, undetermined fragmentations and water clusters also contribute to the uncertainty, though we identified some potential fragments and water clusters through the strength of correlations as previously indicated. We acknowledge that this method cannot identify all fragments and clusters, and fragments and clusters may still be present in the measured VOCs and OVOCs. Further research is needed to explore the impact of fragments and clusters on the measurements, particularly concerning OVOCs with multiple oxygens.

Double bond equivalent (DBE), carbon oxidation state (\overline{OS}_C), and volatility of organic vapors were calculated to address the chemical and physical properties of detected organic vapors (see Text S1). The condensational growth rates contributed by detected organic vapors were simulated using a kinetic partitioning method, as detailed in Li et al. (2024b). For comparison, the condensational growth rates of low volatile and extremely low volatile organic compounds measured by nitrate-CIMS were also simulated (Li et al., 2024b). The OH reactivities of detected organic vapors were calculated, and the rate constants are from Data S1 in Pfannerstill et al. (2024) and Table S4 in Wu et al. (2020). For species with unreported rate constants, we calculated the OH reactivities for hydrocarbons and OVOCs using the reported median rate constants of hydrocarbons and OVOCs, respectively.

Quantified ~~or semi-quantified~~ mixing ratios were further processed by cluster analysis to investigate their characteristics. Intraclass correlation coefficient (ICC) is a suitable method for assessing the consistency of trends in unbalanced data. It quantifies the stability of differences between two sets of measurement results, enabling evaluation of their consistency. ICC combined with k-means cluster analysis were used. ICC(C, 1) was selected among

300 several typical consistency evaluation parameters for its evaluation results
301 exhibit the highest level of differentiation based on factual evidence (Qiao et al.,
302 2021). ICC(C, 1) was calculated as follows:

$$303 \quad ICC(C, 1) = (D(X + Y) - D(X - Y)) / (D(X + Y) + D(X - Y)) \quad (1)$$

304 where $D(\cdot)$ is the arithmetic operators of variance. X and Y are two sets of
305 measurement data, in this case referring to the mixing ratios of any organic
306 vapors we are concerned about. The ICC matrices of various organic vapors
307 were subsequently utilized as input for k-means analysis. Square Euclidean
308 distance was selected to calculate the distances between different organic
309 vapors.

310 **3 Results and discussion**

311 **3.1 General characteristics of organic vapors**

312 During the measurement period, a total of 895 peaks were observed, and 512
313 of them can be assigned to formulae, divided into C_xH_y , $C_xH_yO_z$, $C_xH_yN_i$, and
314 $C_xH_yO_zN_i$ categories based on their elemental compositions (Fig. 1a). $C_xH_yO_z$
315 composes up to 54% of the total number of formulae followed by $C_xH_yO_zN_i$,
316 C_xH_y , and $C_xH_yN_i$, with proportions of 26%, 14%, and 6%, respectively (Fig. 1b).
317 $C_xH_yO_z$ dominates contributing 74% of the annual median mixing ratios of total
318 organics, followed by C_xH_y , $C_xH_yO_zN_i$, and $C_xH_yN_i$, with proportions of 22%, 2%,
319 and 2%, respectively (Fig. 1c). In addition to these resolved formulae, we also
320 detect 18 peaks containing other elements such as S, Cl, Si, etc., and 79
321 CH(O)(N) peaks that do not comply with nitrogen rules, which we consider as
322 fragments or free radicals. Others are unknown peaks for which formulae
323 cannot be assigned or water clusters/fragments excluded from analysis. The
324 mixing ratios of organic vapors vary substantially in urban Beijing, ranging from
325 0.01 parts per trillion (ppt) to 10 parts per billion (ppb) in volume under a time
326 resolution of 1 min, with many species detected at sub-ppt levels notably (Fig.
327 1d). The units of the mixing ratio in the following text are all volume fractions.
328 As the molecular masses of organics increase, their annual median mixing
329 ratios decrease. The mixing ratios of $C_xH_yO_z$ and $C_xH_yO_zN_i$ categories start to
330 decrease below the ppt level above molecular weights of 160 and 125,
331 respectively.

332 With enhanced sensitivity and mass resolution, an increased number of
333 formulae have been identified compared to traditional PTR-MS measurements
334 in urban Beijing, especially formulae with lower mixing ratios and higher oxygen
335 contents. Note that most organics with low mixing ratios have high oxygen
336 content. 44% number of formulae measured in this study are at sub-ppt level
337 while 31% number of formulae are between 1 and 10 ppt (Fig. 1e). Only
338 compounds detected above ppt levels were previously reported in urban sites

339 within Beijing (Sheng et al., 2018; Li et al., 2019), as well as at a suburban site
340 located 100 km southwest of Beijing (He et al., 2022). Simultaneously, organic
341 vapors with multiple oxygens ($C_xH_yO_{\geq 3}$ and $C_xH_yO_{\geq 3}N_i$ species) have been
342 successfully detected in this study in the urban atmosphere. Traditionally, they
343 have been often recognized as total $C_xH_yO_{\geq 3}$ species, with no individual
344 analysis in traditional PTR-MS (Yuan et al., 2023; Li et al., 2022b; He et al.,
345 2022). Many other studies only focus on reporting OVOCs containing up to 2-3
346 oxygens or omit to address the presence of nitrogen containing OVOCs (Wang
347 et al., 2021a; Liu et al., 2022). The low mixing ratios and high wall losses of
348 organic vapors with multiple oxygens impact the detection in traditional PTR-
349 MS (Breitenlechner et al., 2017). [Figure 2a](#) reinterprets the mass defect plot of
350 measured organics with a focus on oxygen numbers, ranging from 0 to 8. The
351 analysis of mixing ratio levels and variations of organic vapors with multiple
352 oxygens (≥ 3) are shown in [Section 3.2](#). Organic vapors with low oxygen content
353 (≤ 2) are reported in [Section 3.3](#). Subsequent comparison of Vocus-PTR and
354 traditional PTR in urban Beijing and both Vocus-PTR measurements in urban
355 Beijing and European forests are also shown in [Section 3.3](#).

356 **3.2 Organic vapors with high oxygen content**

357 195 observed organics with multiple oxygen atoms account for 38% in number
358 of the total organics, including 136 species of $C_xH_yO_{\geq 3}$ and 59 species of
359 $C_xH_yO_{\geq 3}N_i$. Organics with oxygen numbers 3 and 4 dominates within the
360 $C_xH_yO_{\geq 3}$ and $C_xH_yO_{\geq 3}N_i$ species ([Fig. 2b](#) and [Fig. 2c](#)). Organics with oxygen
361 number of 3, 4, 5, and ≥ 6 comprise 15%, 11%, 7%, and 6% of the total species
362 number of $C_xH_yO_z$ compounds, respectively. While compounds with oxygen
363 number of 3, 4, 5, and ≥ 6 comprise 15%, 12%, 7%, and 2% of the total species
364 number of $C_xH_yO_zN_i$ compounds, respectively.

365 The measured organic vapors with multiple oxygens are mainly intermediate
366 volatile organic compounds (IVOCs) and semi-volatile organic compounds
367 (SVOCs). The dominant carbon numbers range from 5 to 9 and DBE between
368 1-5, accounting for over three-quarters of the total species number of organic
369 vapors with multiple oxygens ([Fig. 3a](#) and [Fig. 3b](#)). The maximum occurrence
370 of organic vapors with 3 or 4 oxygen atoms is observed within the carbon range
371 of 7-8 and a DBE value of 2. For organic species with 5 or more oxygens, they
372 reach their peak at a smaller carbon number of 4-5 and a higher DBE value of
373 3. Aromatic VOCs have DBE values no smaller than 4, while aliphatic VOCs
374 usually have DBE values smaller than 2. For organic vapors with DBE between
375 2-3, they are likely oxidation products of aliphatic and aromatic VOCs (Wang et
376 al., 2021b; Nie et al., 2022). For the same number of carbon atoms, organic
377 vapors with a higher number of oxygen atoms exhibit a higher carbon oxidation
378 state (as shown in [Figure S5](#)). Compared to organic vapors with 3 or 4 oxygen
379 atoms, organic vapors with 5 or more oxygens have undergone more extensive

380 atmospheric oxidation and functionalization processes (Kroll et al., 2011;
381 Isaacman-Vanwertz et al., 2018). Based on calculated volatility, 81% of the
382 species are IVOCs, and the remaining 19% are SVOCs (Fig. 3c). With the
383 increase in oxygen number, the volatility of the compounds gradually decreases,
384 while the potential partitioning to aerosols increases, manifested by a gradual
385 reduction in the peak values of the $\log_{10}C_0$. Compounds containing nitrogen,
386 referred to shaded bars with white stripes in Figure 3c, have a lower volatility
387 compared to non-nitrogen species.

388 The annual median mixing ratio of measured organic vapors with multiple
389 oxygens in median \pm standard deviation is 2.0 ppb \pm 1.00.9 ppb, accounting for
390 4% of the total $C_xH_yO_z$ and $C_xH_yO_zN_i$ mixing ratios. For $C_xH_yO_z$ category, the
391 annual median mixing ratios of species with 3, 4, 5, and ≥ 6 oxygens are 1.4
392 ppb, 186.04 ppt, 18.117.8 ppt, and 6.45.9 ppt, respectively. For $C_xH_yO_zN_i$
393 category, the annual median mixing ratios of species with 3, 4, 5, and ≥ 6
394 oxygens are 49.96, 24.5, 2.64, and 0.5 ppt, respectively (Fig. 2d and 2e).
395 Organic vapors with 3 oxygens constitute the overwhelming majority of the
396 mixing ratio of measured organic vapors with more than three oxygens. As a
397 result, the mixing ratio-weighted carbon number and DBE distributions (Fig. 3d
398 and Fig. 3e) are significantly different from that of species number distributions
399 for organic vapors with multiple oxygens. The mixing ratios of species with
400 carbon numbers ranging from 2 to 6 are significantly higher, with those
401 containing four carbons exhibiting the highest mixing ratios. Similarly, the
402 mixing ratios of species with DBE ranging from 0-4 are notably higher than that
403 of other DBE values. As compounds containing 3 oxygens dominate the mixing
404 ratio, IVOCs nearly entirely contribute to the mixing ratio-weighted volatility of
405 organic vapors with multiple oxygens (Fig. 3f). The mixing ratios of organic
406 vapors with multiple oxygens measured in this study are higher than other
407 studies, which will be detailed in Section 3.3.

408 Though the contribution of the measured IVOCs and SVOCs to the overall VOC
409 mixing ratio is low, their contribution to the condensational growth rates is non-
410 negligible, which may influence the growth of new particles (Ehn et al., 2014),
411 SOA formation (Jimenez et al., 2009), and haze (Nie et al., 2022). The
412 condensational growth rates of total organic vapors are calculated, including
413 extremely low, low, and semi volatile organic compounds detected by nitrate-
414 CIMS and I/SVOCs detected by Vocus-PTR. The contribution to the
415 condensational growth rate from I/SVOCs detected by Vocus-PTR increases
416 with particle size and decreases with temperature. For 8 nm particles, the
417 contribution of SVOCs detected by Vocus-PTR is 9%, while IVOCs contribute
418 1%. For 40 nm particles, the contribution of SVOCs increases to 13%, and
419 IVOCs rise to 4%. At sub-zero temperatures for 8 nm particles, the SVOC
420 contribution detected by Vocus-PTR can reach up to 21%, with IVOCs
421 contributing 10%.

422 The molecular formulae of the measured organic vapors with multiple oxygens
423 are displayed in the mass spectra, categorized by carbon numbers ranging from
424 2-11 (Fig. 4 and Table S3S4). Many of the formulae are reported as oxidation
425 products of various VOC precursors in previous studies. Take isoprene as an
426 example, detected formulae are reported as various oxidation products of
427 isoprene, including $C_5H_{10}O_3$ and subsequent oxidation products in C5 species,
428 e.g., $C_5H_8O_6$, $C_5H_9NO_4$, etc. (Wennberg et al., 2018). For several C4 species,
429 such as $C_4H_7NO_4$, $C_4H_4O_3$, etc., they are reported as oxidation products of two
430 additional important oxidation products of isoprene, methacrolein (MACR) and
431 methyl vinyl ketone (MVK). We also see formulae reported as oxidation
432 products of precursors such as benzene (C6) (Priestley et al., 2021), alkyl-
433 substituted benzenes (C7-C9) (Pan and Wang, 2014; Wang et al., 2020c;
434 Cheng et al., 2021), and monoterpenes (C10) (Rolletter et al., 2019). Besides,
435 we can also detect some organic vapors with relatively low DBE (≤ 3), which
436 may originate from the oxidation of aliphatic precursors. For example, $C_5H_8O_4$
437 observed are reported as one of the oxidation products of C5 aldehyde, the
438 photolysis of which release OH radicals. This mechanism may explain the
439 source gap of OH radicals between simulations and observations in low
440 nitrogen oxide and high VOCs regimes (Yang et al., 2024). Note that these
441 species may be oxidation products as reported by previous studies; however,
442 confirming this would require additional techniques such as GC.

443 Measured molecular formulae may react with OH radicals, contributing to OH
444 reactivity. The calculated OH reactivity of organic vapors with multiple oxygens
445 account for 6% of the total detected VOCs, with an average annual value of 1.2
446 s^{-1} . Previous studies show differences between measured and calculated or
447 modeled OH reactivity (Hansen et al., 2014), and unmeasured species from
448 photochemical oxidation likely explain this gap (Ferracci et al., 2018). Therefore,
449 the OH reactivity contributed by detected organic vapors with multiple oxygens
450 in this study may potentially reduce this gap, thereby improve the accuracy of
451 diagnosis of sensitivity regimes for ozone formation (Wang et al., 2024). Using
452 Vocus-PTR has the potential to simultaneously measure both precursors and
453 multi-generational oxygenated products, which is beneficial for studying the
454 evolution process of organic compounds in the atmosphere.

455 As for the seasonal variations, the overall mixing ratio of organic vapors with
456 multiple oxygens is the highest in winter, followed by summer, spring and the
457 lowest in autumn (Fig. 5a). The mixing ratios expressed in median \pm standard
458 deviation (ppb \pm ppb) are 1.9 ± 0.5 , 1.9 ± 0.9 , 1.4 ± 1.2 , and 2.2 ± 0.8 for spring,
459 summer, autumn, and winter, respectively. Compounds with different oxygens
460 exhibit different seasonal variations, shown in Figure 5b and 5c and Table S4S5.
461 For $C_xH_yO_z$ with 3 or 4 oxygens, the mixing ratios are higher in winter than in
462 other seasons, while for compounds containing 5 or more oxygens, the mixing
463 ratios are highest in summer. For $C_xH_yO_zN_i$ with 3 or 4 oxygens, the mixing

464 ratios are high in both summer and winter, while for compounds containing 5 or
465 more oxygens, the mixing ratios are high in summer and spring. As the oxygen
466 number increases, the contribution from secondary sources becomes greater,
467 and the high mixing ratio of oxidants in summer intensifies this process. Thus,
468 the fraction of the mixing ratio of compounds with multiple oxygens increases
469 with the oxygen number in summer (Fig. 5d). In winter, the mixing ratios of
470 compounds containing five or more oxygens are substantially suppressed,
471 which may be due to reduced generation. Alternatively, it could be that these
472 compounds belong to SVOCs, with a majority being partitioned onto particulate
473 matter at low temperatures.

474 The seasonal variations of organic vapors with multiple oxygens differ from
475 those of total OVOCs (Fig. S6), with the latter's mixing ratio being primarily
476 influenced by organic vapors containing 1-2 oxygen atoms. The mixing ratio of
477 total OVOCs in winter is substantially higher than in the other three seasons,
478 followed by autumn and summer, with the lowest mixing ratio observed in spring.
479 The seasonal variations of OVOCs are partly caused by the variation of mixing
480 layer height (Li et al., 2023), which is lowest in winter. Cluster analysis is
481 performed to further explore the dominated driving factors of the seasonal
482 variations of organic vapors with multiple oxygens. Three clusters are identified
483 in each season based on the diurnal profiles of each compound. To increase
484 the interpretability of the clusters, two of them are merged. Figure 6 and Figure
485 S7 shows the cluster results for organic vapors with multiple oxygens. For
486 comparison, cluster analysis is performed on organic vapors with 1-2 oxygens
487 as well (Fig. S8 and Fig. S9).

488 Daytime clusters, where the peak occurs during the daytime, were identified
489 across the four seasons for organic vapors with multiple oxygens (shown as
490 cluster 1 in Fig. 6). Daytime clusters start to rise at 6:00-7:00 (6:00 for summer
491 and 7:00 for other seasons), peak at 11:00-14:00 and then slowly decrease,
492 following the diurnal variation of solar radiation (Li et al., 2023), ozone and
493 temperature (Fig. S2). Figure S10 further demonstrates the dependence of
494 daytime clusters on temperature. The mixing ratio of daytime clusters show an
495 apparent increase in summer (when temperature is higher than 15 °C), which
496 indicates that higher temperatures accompanied by an increase in solar
497 radiation and ozone favors the formation of daytime clusters. The number and
498 corresponding mixing ratios of species allocated to the daytime clusters vary in
499 four seasons. In summer, the vast majority of species (~~7776~~%) exhibit daytime
500 characteristics, with a mixing ratio percentage as high as ~~8582~~%, which may
501 be related to the strongest solar radiation (Li et al., 2023) and lowest NO_x
502 concentrations (Fig. S2). The contribution of daytime clusters in autumn is also
503 significant, with ~~6768~~% and ~~5861~~% of the species and mixing ratios being
504 accounted for. The noon peaks of daytime clusters in winter and spring are
505 relatively less pronounced, with the species and mixing ratio day/night ratios

506 also being comparatively lower. The afternoon peak of daytime clusters in
507 autumn and winter are accompanied by a decrease in mixing layer height (Li et
508 al., 2023). For organic vapors with 1 or 2 oxygens, a significant daytime cluster
509 was observed only in summer (Fig. S8 d-f).

510 Another cluster type is considered to be nighttime clusters, as the
511 corresponding species have their highest mixing ratios at night. Unlike the
512 daytime cluster, the diurnal variations of nighttime clusters are different in four
513 seasons (Fig. 6). In spring, the nighttime cluster comprises over ~~8687~~⁸⁶⁸⁷% of
514 ~~nighttime~~-species and ~~7775~~⁷⁷⁷⁵% of mixing ratios, and it peaks at 4:00 with low
515 daytime values. The nighttime clusters in winter and autumn show bimodal
516 diurnal variations, with the highest peak occurring during the night from 19:00
517 to 23:00, and the second peak appearing during the day from 8:00 to 12:00.
518 ~~4745~~⁴⁷⁴⁵% and ~~3332~~³³³²% of species exhibit the characteristics of the nighttime cluster
519 in winter and autumn, constituting ~~5859~~⁵⁸⁵⁹% and ~~4239~~⁴²³⁹% of the mixing ratio,
520 respectively. The contribution of the nighttime cluster is minimal in summer,
521 reaching its peak at midnight. We found that each nighttime cluster of organic
522 vapors with multiple oxygens shows good consistency with the corresponding
523 major clusters of organic vapors containing 1-2 oxygens (Fig. S8 and Fig. S11),
524 while the mixing ratios during midday differ. Nighttime clusters also show better
525 consistency with PM_{2.5} compared to daytime clusters (Fig. S2), which may be
526 related to mixed sources.

527 Most organic vapors with multiple oxygens could be assigned to different
528 clusters in different seasons (Fig. S12). Only a small number of species can be
529 categorized into the same cluster in four seasons. Figure S13 shows the
530 average C, H, O, and N number of species assigned to daytime cluster 0-4
531 times during the four seasons. As compounds exhibit more characteristics
532 associated with daytime cluster, there is no significant change in the carbon
533 number, but there is an increase in hydrogen and oxygen number, and a
534 decrease in nitrogen number. This may be due to multi-step oxidation reactions
535 in the atmosphere, causing an increase in oxygen number and DBE of species
536 (Kroll et al., 2011; Isaacman-Vanwertz et al., 2018), with diurnal variations
537 peaking at noon as a result of the strongest photochemistry. The decreasing
538 trend of the number of nitrogen atoms in Figure S13 indicates that nitrogen
539 containing compounds measured in this study are more likely to come from
540 nocturnal production or emissions. Regarding the average elemental
541 composition (C, H, O, and N) of species assigned to two clusters (see Fig. S14),
542 daytime clusters typically exhibit higher oxygen content and lower H/C
543 compared to nighttime clusters, providing further evidence supporting the
544 atmospheric photochemical origin of daytime clusters. The nighttime clusters
545 have higher nitrogen contents than daytime clusters, indicating more of the
546 impacts of nocturnal sources.

547 3.3 Organic vapors with low oxygen content

548 In addition to multiple oxygens, organic vapors with low oxygen content were
549 also measured in urban Beijing in this study. Here we primarily discuss
550 comparisons between the results of this study and those of previous studies.
551 The mixing ratios and variations of typical VOCs measured in this study are
552 comparable to the results obtained by traditional PTR-MS measurements in
553 both urban Beijing and neighboring regions. [Figure S15](#) shows the diurnal
554 profiles of 12 representative VOCs in four seasons. OVOCs of C_2H_4O , C_3H_6O ,
555 and C_4H_4O , usually identified as acetaldehyde, acetone, and furan, are mainly
556 from anthropogenic sources as reported by previous studies (Qian et al., 2019).
557 Their diurnal variations exhibit a characteristic of being higher at night and lower
558 during the day, similar to other studies reported in Beijing during the winter
559 (Sheng et al., 2018; He et al., 2022). The mixing ratios of acetaldehyde, methyl
560 ethyl ketone (MEK), and furan in winter are slightly lower than those observed
561 in winter Beijing in 2016 and 2018 (Sheng et al., 2018; He et al., 2022). The
562 winter mixing ratios of acetone are higher than other seasons and observed in
563 other studies, indicating an unknown emission source during winter. The mixing
564 ratios of benzene (C_6H_6), toluene (C_7H_8), and naphthalene ($C_{10}H_8$) in winter are
565 slightly lower than reported in winter in Beijing during the past few years (Sheng
566 et al., 2018; Li et al., 2019; He et al., 2022), possibly due to improvements in
567 air pollution policies, especially those targeting emissions from residential
568 combustion and motor vehicles (Liu et al., 2023). As for phenols, the mixing
569 ratios of C_6H_6O are similar to measurement at a background site in the North
570 China Plain in winter, while the mixing ratios of C_7H_8O are much lower than that
571 (He et al., 2022). High mixing ratios of biogenic emissions in summer are
572 observed, for example isoprene (C_5H_8) and the sum of its oxidation products
573 MACR and MVK (Apel et al., 2002) have peak mixing ratios of 2.6 ppb and 0.6
574 ppb, respectively. Their mixing ratios in winter are lower and consistent with
575 other studies (Sheng et al., 2018; He et al., 2022).

576 The mixing ratio fractions of organic categories in urban Beijing using Vocus-
577 PTR differ from the results obtained using traditional PTR-MS. Previous studies
578 in Beijing have only reported a few selected VOCs up to around 100 species,
579 resulting in limited results on systematic characterizations of VOCs using PTR-
580 MS in Beijing (Sheng et al., 2018; Li et al., 2019; Wang et al., 2021a; Liu et al.,
581 2022). Therefore, we compare with a suburban site, Gucheng, which is located
582 100 km southwest from our site. The two sites (urban Beijing and Gucheng) are
583 both located in the North China Plain and are subject to regional air pollutions
584 simultaneously. [Figure S16](#) shows the comparison results of five categories,
585 including C_xH_y , C_xH_yO , $C_xH_yO_2$, $C_xH_yO_{\geq 3}$, and N/S containing compounds. The
586 first difference is that the mixing ratio fraction of species containing two or more
587 oxygens measured by Vocus-PTR is higher than those measured by traditional
588 PTR-MS. The mixing ratio fractions of $C_xH_yO_2$ and $C_xH_yO_{\geq 3}$ in Vocus-PTR are

589 12% and 4%, respectively, whereas they are 6% and 1% for traditional PTR-
590 MS. In terms of mixing ratios, the mixing ratio of $C_xH_yO_{\geq 3}$ is approximately
591 double in Vocus-PTR compared to traditional PTR-MS, while the mixing ratio of
592 C_xH_yO is half compared to traditional PTR-MS measurement. The mixing ratio
593 of $C_xH_yO_2$ remains similar. This is because Vocus-PTR can detect more OVOCs
594 with multiple oxygens due to its high sensitivity and mass resolution, whereas
595 due to its low transmission efficiency for low masses, it is difficult to detect high
596 mixing ratio OVOCs such as methanol and formaldehyde. The other difference
597 is that the mixing ratio and the corresponding fraction of C_xH_y species measured
598 by Vocus-PTR are much lower than those measured by traditional PTR. For
599 several major C_xH_y compounds such as benzene, C7, C8, and C9 aromatics,
600 their mixing ratios are comparable between the two methods. The main
601 difference between the two methods lies in the mixing ratio of low-mass
602 hydrocarbons. Overall, when applied to the urban atmosphere, Vocus-PTR has
603 advantages in measuring oxygenated VOCs, especially with multiple oxygens.
604 However, it has limitations in measuring low molecular weight VOCs due to the
605 low-mass cutoff in the transmission efficiency.

606 The molecular characteristics of organic vapors measured by Vocus-PTR in
607 urban Beijing show several differences from those in forested areas (Li et al.,
608 2020; Huang et al., 2021; Li et al., 2021). Firstly, organics up to 300 m/z can be
609 observed in forested areas, while organics up to 230 m/z are observed (Fig.
610 1a). Two main reasons are responsible for this. The complexity of the species
611 introduces challenges in interpreting mass spectra, which is evidenced by the
612 total number of species being similar to existing atmospheric measurements
613 using Vocus-PTR, despite a narrower mass range in this study. The higher
614 particulate matter concentrations in urban areas provide a larger sink for
615 organic vapors (Deng et al., 2020), and this loss effect is especially pronounced
616 for compounds with high molecular weights due to their lower volatility. The
617 second difference is that, $C_xH_yO_z$ and $C_xH_yO_zN_i$ species are the dominant
618 organics in both urban and forested areas, whilst $C_xH_yN_i$ species are more
619 common and abundant in urban areas, which may come from biomass burning
620 emissions (Laskin et al., 2009). Thirdly, VOCs with low carbon and oxygen
621 number play a more significant role in total organic mixing ratio compared to
622 results from forested regions. As shown in Figure S17a, C_2 and C_3 organics
623 contribute 79% of the total organic mixing ratio in this study, while C_4 - C_6
624 organics contribute approximately 75% in forested regions. In contrast to
625 forested areas, where VOCs and IVOCs mixing ratios are comparable, the
626 majority of the total organic mixing ratio is attributed to VOCs in this study (Fig.
627 S17b). Typical C_2 and C_3 organics, such as C_3H_6O , C_2H_4O , and $C_2H_4O_2$,
628 contribute 14%, 11%, and 5%, respectively, to the total organic mixing ratio,
629 which are mainly originated from anthropogenic emissions including industrial
630 and vehicular activities, solvent utilization, and other sources (Qian et al., 2019).

631 **4 Conclusions**

632 In this study, we explore the molecular and seasonal characteristics of organic
633 vapors in urban Beijing using a Vocus-PTR over four seasons. A total of 895
634 peaks are observed, and 512 of them can be assigned to formulae. The
635 contribution of $C_xH_yO_z$ species is most significant, which compose up to 54% of
636 the number and 74% of the mixing ratios of total organics. With enhanced
637 sensitivity and mass resolution, an increased number of species were observed
638 compared to traditional PTR-MS measurements in urban Beijing, especially
639 compounds with lower mixing ratios and higher oxygen content. 44% species
640 in number measured in this study are at sub-ppt level and 3138% species in
641 number contain 3-8 oxygens, resulting in a higher fraction of species containing
642 three or more oxygens compared to traditional PTR-MS measurements.
643 Organic vapors with low oxygen content are comparable to those obtained in
644 both urban Beijing and neighboring regions, and they exert a more substantial
645 influence on the overall organic mixing in forested areas.

646 The mixing ratio of organic vapors with multiple oxygens accounts for 4% of the
647 total VOC mixing ratio, with the highest levels observed in winter, followed by
648 summer, spring, and the lowest in autumn. These vapors also make a non-
649 negligible contribution to condensational growth and OH reactivity. In summer,
650 the majority of species are aligned to daytime cluster (peaking at noon),
651 primarily originating from the photooxidation process. As the oxygen number
652 increases, the impact of the photooxidation process becomes more
653 pronounced, leading to an increase in both mixing ratio and proportion of
654 organic vapors with multiple oxygens during summer. In spring and winter when
655 the nighttime cluster (peaking at night) dominated, the variations of organic
656 vapors with multiple oxygens are strongly correlated with organic vapors with
657 one or two oxygens. The measured compositions and seasonal variabilities of
658 organic vapors with multiple oxygens emphasize the importance of high
659 sensitivity and high mass resolution measurements in urban atmosphere,
660 suggesting prospective for future research.

661 **Data availability**

662 Data are available upon request from the corresponding author.

663 **Supporting Information**

664 The content of the SI includes the map of the observation site (Fig. S1); the
665 diurnal variations of $PM_{2.5}$, O_3 , NO_x , RH, and T in four seasons (Fig. S2);
666 calibration results of mixed calibration gases (Fig. S3); average limits of
667 detection (1 min) for detected compounds (Fig. S4); carbon oxidation state of

668 organic vapors with different oxygens (Fig. S5); boxplot of total OVOC mixing
669 ratios in four seasons (Fig. S6); diurnal variation cluster results of organic
670 vapors with multiple oxygens (Fig. S7); cluster results of organic vapors with
671 one or two oxygens (Fig. S8-S9); dependence of daytime clusters on
672 temperature (Fig. S10); dependence of nighttime clusters on major clusters of
673 organic vapors with 1-2 oxygens (Fig. S11); the distribution of organic vapors
674 with multiple oxygens across different clusters (Fig. S12); average C, H, O, and
675 N number of organic vapors containing multiple oxygens with different diurnal
676 patterns (Fig. S13); average C, H, O, and N number of organic vapors
677 containing multiple oxygens in two clusters (Fig. S14); diurnal profiles of
678 representative VOCs in four seasons (Fig. S15); comparison results with
679 Gucheng site (Fig. S16); molecular characteristics of total measured organic
680 vapors by Vocus-PTR (Fig. S17); the observation periods of Vocus-PTR (Table
681 S1); information about calibration gases (Table S2); [corrected fragments and](#)
682 [water clusters \(Table S3\)](#); main $C_xH_yO_{\geq 3}$ and $C_xH_yO_{\geq 3}N$ species measured in
683 this study (Table [S3S4](#)), and seasonal mixing ratios of OVOCs with multiple
684 oxygens (Table [S4S5](#)).

685 **Author contributions**

686 Conceptualization: JJ and ZA. Data collection and analysis: ZA, RY, XZ, XxL,
687 YY, JG, YuL, YZ, and XuL. Writing-original draft: ZA. Writing-review and editing:
688 XxL, DL, YaL, DW, CY, KH, DRW, FNK, and JJ.

689 **Competing interests**

690 At least one of the (co-)authors is a member of the editorial board of
691 *Atmospheric Chemistry and Physics*.

692 **Financial support**

693 This work has been supported by the National Natural Science Foundation of
694 China (Grant NO. 22206097, 22188102, and 22106083) and Samsung PM_{2.5}
695 SRP.

696 **References**

697 Apel, E. C., Riemer, D. D., Hills, A., Baugh, W., Orlando, J., Faloon, I., Tan, D.,
698 Brune, W., Lamb, B., Westberg, H., Carroll, M. A., Thornberry, T., and Geron,
699 C. D.: Measurement and interpretation of isoprene fluxes and isoprene,
700 methacrolein, and methyl vinyl ketone mixing ratios at the PROPHET site
701 during the 1998 Intensive, *J. Geophys. Res.: Atmos.*, 107,
702 10.1029/2000jd000225, 2002.

703 Bianchi, F., Kurten, T., Riva, M., Mohr, C., Rissanen, M. P., Roldin, P., Berndt,
704 T., Crouse, J. D., Wennberg, P. O., Mentel, T. F., Wildt, J., Junninen, H.,
705 Jokinen, T., Kulmala, M., Worsnop, D. R., Thornton, J. A., Donahue, N.,
706 Kjaergaard, H. G., and Ehn, M.: Highly Oxygenated Organic Molecules (HOM)
707 from Gas-Phase Autoxidation Involving Peroxy Radicals: A Key Contributor to
708 Atmospheric Aerosol, *Chem. Rev.*, 119, 3472-3509,
709 10.1021/acs.chemrev.8b00395, 2019.

710 Breitenlechner, M., Fischer, L., Hainer, M., Heinritzi, M., Curtius, J., and Hansel,
711 A.: PTR3: An Instrument for Studying the Lifecycle of Reactive Organic Carbon
712 in the Atmosphere, *Anal Chem*, 89, 5824-5831,
713 10.1021/acs.analchem.6b05110, 2017.

714 Cai, R. and Jiang, J.: A new balance formula to estimate new particle formation
715 rate: reevaluating the effect of coagulation scavenging, *Atmos. Chem. Phys.*,
716 17, 12659-12675, 10.5194/acp-17-12659-2017, 2017.

717 Cappellin, L., Karl, T., Probst, M., Ismailova, O., Winkler, P. M., Soukoulis, C.,
718 Aprea, E., Mark, T. D., Gasperi, F., and Biasioli, F.: On quantitative
719 determination of volatile organic compound concentrations using proton
720 transfer reaction time-of-flight mass spectrometry, *Environ Sci Technol*, 46,
721 2283-2290, 10.1021/es203985t, 2012.

722 Carter, W. P. L.: Development of Ozone Reactivity Scales for Volatile Organic
723 Compounds, *Air & Waste*, 44, 881-899, 10.1080/1073161X.1994.10467290,
724 1994.

725 Chang, Y., Wang, H., Gao, Y., Jing, S., Lu, Y., Lou, S., Kuang, Y., Cheng, K.,
726 Ling, Q., Zhu, L., Tan, W., and Huang, R. J.: Nonagricultural emissions
727 dominate urban atmospheric amines as revealed by mobile measurements,
728 *Geophys. Res. Lett.*, 10.1029/2021gl097640, 2022.

729 Cheng, X., Chen, Q., Jie Li, Y., Zheng, Y., Liao, K., and Huang, G.: Highly
730 oxygenated organic molecules produced by the oxidation of benzene and
731 toluene in a wide range of OH exposure and NO_x conditions, *Atmos. Chem.*
732 *Phys.*, 21, 12005-12019, 10.5194/acp-21-12005-2021, 2021.

733 Coggon, M. M., Stockwell, C. E., Clafin, M. S., Pfannerstill, E. Y., Xu, L., Gilman,
734 J. B., Marcantonio, J., Cao, C., Bates, K., Gkatzelis, G. I., Lamplugh, A., Katz,
735 E. F., Arata, C., Apel, E. C., Hornbrook, R. S., Piel, F., Majluf, F., Blake, D. R.,
736 Wisthaler, A., Canagaratna, M., Lerner, B. M., Goldstein, A. H., Mak, J. E., and
737 Warneke, C.: Identifying and correcting interferences to PTR-ToF-MS
738 measurements of isoprene and other urban volatile organic compounds, *Atmos.*
739 *Meas. Tech.*, 17, 801-825, 10.5194/amt-17-801-2024, 2024.

740 de Gouw, J. and Warneke, C.: Measurements of volatile organic compounds in
741 the earth's atmosphere using proton-transfer-reaction mass spectrometry,
742 *Mass Spectrom Rev*, 26, 223-257, 10.1002/mas.20119, 2007.

743 Deng, C., Fu, Y., Dada, L., Yan, C., Cai, R., Yang, D., Zhou, Y., Yin, R., Lu, Y.,
744 Li, X., Qiao, X., Fan, X., Nie, W., Kontkanen, J., Kangasluoma, J., Chu, B., Ding,
745 A., Kerminen, V. M., Paasonen, P., Worsnop, D. R., Bianchi, F., Liu, Y., Zheng,
746 J., Wang, L., Kulmala, M., and Jiang, J.: Seasonal Characteristics of New
747 Particle Formation and Growth in Urban Beijing, *Environ Sci Technol*, 54, 8547-
748 8557, 10.1021/acs.est.0c00808, 2020.

749 Ehn, M., Thornton, J. A., Kleist, E., Sipilä, M., Junninen, H., Pullinen, I., Springer,
750 M., Rubach, F., Tillmann, R., Lee, B., Lopez-Hilfiker, F., Andres, S., Acir, I.-H.,
751 Rissanen, M., Jokinen, T., Schobesberger, S., Kangasluoma, J., Kontkanen, J.,
752 Nieminen, T., Kurtén, T., Nielsen, L. B., Jørgensen, S., Kjaergaard, H. G.,
753 Canagaratna, M., Maso, M. D., Berndt, T., Petäjä, T., Wahner, A., Kerminen, V.-

- 754 M., Kulmala, M., Worsnop, D. R., Wildt, J., and Mentel, T. F.: A large source of
755 low-volatility secondary organic aerosol, *Nature*, 506, 476-479,
756 10.1038/nature13032, 2014.
- 757 Ferracci, V., Heimann, I., Abraham, N. L., Pyle, J. A., and Archibald, A. T.: Global
758 modelling of the total OH reactivity: investigations on the “missing” OH sink and
759 its atmospheric implications, *Atmos. Chem. Phys.*, 18, 7109-7129,
760 10.5194/acp-18-7109-2018, 2018.
- 761 Fischer, L., Breitenlechner, M., Canaval, E., Scholz, W., Striednig, M., Graus,
762 M., Karl, T. G., Petäjä, T., Kulmala, M., and Hansel, A.: First eddy covariance
763 flux measurements of semi-volatile organic compounds with the PTR3-TOF-
764 MS, *Atmos. Meas. Tech.*, 14, 8019-8039, 10.5194/amt-14-8019-2021, 2021.
- 765 Gentner, D. R., Worton, D. R., Isaacman, G., Davis, L. C., Dallmann, T. R.,
766 Wood, E. C., Herndon, S. C., Goldstein, A. H., and Harley, R. A.: Chemical
767 Composition of Gas-Phase Organic Carbon Emissions from Motor Vehicles and
768 Implications for Ozone Production, *Environ. Sci. Technol.*, 47, 11837-11848,
769 10.1021/es401470e, 2013.
- 770 Gilman, J. B., Lerner, B. M., Kuster, W. C., Goldan, P. D., Warneke, C., Veres,
771 P. R., Roberts, J. M., de Gouw, J. A., Burling, I. R., and Yokelson, R. J.: Biomass
772 burning emissions and potential air quality impacts of volatile organic
773 compounds and other trace gases from fuels common in the US, *Atmos. Chem.*
774 *Phys.*, 15, 13915-13938, 10.5194/acp-15-13915-2015, 2015.
- 775 Goldstein, A. H. and Galbally, I. E.: Known and Unexplored Organic
776 Constituents in the Earth's Atmosphere, *Environ. Sci. Technol.*, 41, 1514-1521,
777 10.1021/es072476p, 2007.
- 778 Gueneron, M., Erickson, M. H., VanderSchelden, G. S., and Jobson, B. T.: PTR-
779 MS fragmentation patterns of gasoline hydrocarbons, *Int. J. Mass Spectrom.*,
780 379, 97-109, 10.1016/j.ijms.2015.01.001, 2015.
- 781 Hallquist, M., Wenger, J. C., Baltensperger, U., Rudich, Y., Simpson, D., Claeys,
782 M., Dommen, J., Donahue, N. M., George, C., Goldstein, A. H., Hamilton, J. F.,
783 Herrmann, H., Hoffmann, T., Iinuma, Y., Jang, M., Jenkin, M. E., Jimenez, J. L.,
784 Kiendler-Scharr, A., Maenhaut, W., McFiggans, G., Mentel, T. F., Monod, A.,
785 Prévôt, A. S. H., Seinfeld, J. H., Surratt, J. D., Szmigielski, R., and Wildt, J.: The
786 formation, properties and impact of secondary organic aerosol: current and
787 emerging issues, *Atmos. Chem. Phys.*, 9, 5155-5236, 10.5194/acp-9-5155-
788 2009, 2009.
- 789 Hansel, A., Jordan, A., Holzinger, R., Prazeller, P., Vogel, W., and Lindinger, W.:
790 Proton transfer reaction mass spectrometry: on-line trace gas analysis at the
791 ppb level, *International Journal of Mass Spectrometry and Ion Processes*, 149-
792 150, 609-619, [https://doi.org/10.1016/0168-1176\(95\)04294-U](https://doi.org/10.1016/0168-1176(95)04294-U), 1995.
- 793 Hansen, R. F., Griffith, S. M., Dusanter, S., Rickly, P. S., Stevens, P. S., Bertman,
794 S. B., Carroll, M. A., Erickson, M. H., Flynn, J. H., Grossberg, N., Jobson, B. T.,
795 Lefer, B. L., and Wallace, H. W.: Measurements of total hydroxyl radical
796 reactivity during CABINEX 2009 – Part 1: field measurements, *Atmos.*
797 *Chem. Phys.*, 14, 2923-2937, 10.5194/acp-14-2923-2014, 2014.
- 798 He, X., Yuan, B., Wu, C., Wang, S., Wang, C., Huangfu, Y., Qi, J., Ma, N., Xu,
799 W., Wang, M., Chen, W., Su, H., Cheng, Y., and Shao, M.: Volatile organic
800 compounds in wintertime North China Plain: Insights from measurements of
801 proton transfer reaction time-of-flight mass spectrometer (PTR-ToF-MS),
802 *Journal of Environmental Sciences*, 10.1016/j.jes.2021.08.010, 2022.
- 803 Huang, W., Li, H., Sarnela, N., Heikkinen, L., Tham, Y. J., Mikkilä, J., Thomas,

804 S. J., Donahue, N. M., Kulmala, M., and Bianchi, F.: Measurement report:
805 Molecular composition and volatility of gaseous organic compounds in a boreal
806 forest – from volatile organic compounds to highly oxygenated organic
807 molecules, *Atmos. Chem. Phys.*, 21, 8961-8977, 10.5194/acp-21-8961-2021,
808 2021.

809 Isaacman-VanWertz, G., Massoli, P., O'Brien, R., Lim, C., Franklin, J. P., Moss,
810 J. A., Hunter, J. F., Nowak, J. B., Canagaratna, M. R., Misztal, P. K., Arata, C.,
811 Roscioli, J. R., Herndon, S. T., Onasch, T. B., Lambe, A. T., Jayne, J. T., Su, L.,
812 Knopf, D. A., Goldstein, A. H., Worsnop, D. R., and Kroll, J. H.: Chemical
813 evolution of atmospheric organic carbon over multiple generations of oxidation,
814 *Nat Chem*, 10, 462-468, 10.1038/s41557-018-0002-2, 2018.

815 Jahn, L. G., Tang, M., Blomdahl, D., Bhattacharyya, N., Abue, P., Novoselac, A.,
816 Ruiz, L. H., and Misztal, P. K.: Volatile organic compound (VOC) emissions from
817 the usage of benzalkonium chloride and other disinfectants based on
818 quaternary ammonium compounds, *Environmental Science: Atmospheres*, 3,
819 363-373, 10.1039/d2ea00054g, 2023.

820 Jensen, A. R., Koss, A. R., Hales, R. B., and de Gouw, J. A.: Measurements of
821 volatile organic compounds in ambient air by gas-chromatography and real-
822 time Vocus PTR-TOF-MS: calibrations, instrument background corrections, and
823 introducing a PTR Data Toolkit, *Atmos. Meas. Tech.*, 16, 5261-5285,
824 10.5194/amt-16-5261-2023, 2023.

825 Jimenez, J. L., Canagaratna, M. R., Donahue, N. M., Prevot, A. S. H., Zhang,
826 Q., Kroll, J. H., DeCarlo, P. F., Allan, J. D., Coe, H., Ng, N. L., Aiken, A. C.,
827 Docherty, K. S., Ulbrich, I. M., Grieshop, A. P., Robinson, A. L., Duplissy, J.,
828 Smith, J. D., Wilson, K. R., Lanz, V. A., Hueglin, C., Sun, Y. L., Tian, J.,
829 Laaksonen, A., Raatikainen, T., Rautiainen, J., Vaattovaara, P., Ehn, M.,
830 Kulmala, M., Tomlinson, J. M., Collins, D. R., Cubison, M. J., Dunlea, E. J.,
831 Huffman, J. A., Onasch, T. B., Alfarra, M. R., Williams, P. I., Bower, K., Kondo,
832 Y., Schneider, J., Drewnick, F., Borrmann, S., Weimer, S., Demerjian, K.,
833 Salcedo, D., Cottrell, L., Griffin, R., Takami, A., Miyoshi, T., Hatakeyama, S.,
834 Shimono, A., Sun, J. Y., Zhang, Y. M., Dzepina, K., Kimmel, J. R., Sueper, D.,
835 Jayne, J. T., Herndon, S. C., Trimborn, A. M., Williams, L. R., Wood, E. C.,
836 Middlebrook, A. M., Kolb, C. E., Baltensperger, U., and Worsnop, D. R.:
837 Evolution of Organic Aerosols in the Atmosphere, *Science*, 326, 1525-1529,
838 10.1126/science.1180353, 2009.

839 Krechmer, J., Lopez-Hilfiker, F., Koss, A., Hutterli, M., Stoermer, C., Deming, B.,
840 Kimmel, J., Warneke, C., Holzinger, R., Jayne, J., Worsnop, D., Fuhrer, K.,
841 Gonin, M., and de Gouw, J.: Evaluation of a New Reagent-Ion Source and
842 Focusing Ion-Molecule Reactor for Use in Proton-Transfer-Reaction Mass
843 Spectrometry, *Anal Chem*, 90, 12011-12018, 10.1021/acs.analchem.8b02641,
844 2018.

845 Kroll, J. H., Donahue, N. M., Jimenez, J. L., Kessler, S. H., Canagaratna, M. R.,
846 Wilson, K. R., Altieri, K. E., Mazzoleni, L. R., Wozniak, A. S., Bluhm, H., Mysak,
847 E. R., Smith, J. D., Kolb, C. E., and Worsnop, D. R.: Carbon oxidation state as
848 a metric for describing the chemistry of atmospheric organic aerosol, *Nature*
849 *Chemistry*, 3, 133-139, 10.1038/nchem.948, 2011.

850 Laskin, A., Smith, J. S., and Laskin, J.: Molecular Characterization of Nitrogen-
851 Containing Organic Compounds in Biomass Burning Aerosols Using High-
852 Resolution Mass Spectrometry, *Environ. Sci. Technol.*, 43, 3764-3771,
853 10.1021/es803456n, 2009.

854 Lewis, A. C., Carslaw, N., Marriott, P. J., Kinghorn, R. M., Morrison, P., Lee, A.
855 L., Bartle, K. D., and Pilling, M. J.: A larger pool of ozone-forming carbon

856 compounds in urban atmospheres, *Nature*, 405, 778-781, 2000.

857 Li, H., Almeida, T. G., Luo, Y., Zhao, J., Palm, B. B., Daub, C. D., Huang, W.,
858 Mohr, C., Krechmer, J. E., Kurtén, T., and Ehn, M.: Fragmentation inside proton-
859 transfer-reaction-based mass spectrometers limits the detection of ROOR and
860 ROOH peroxides, *Atmos. Meas. Tech.*, 15, 1811-1827, 10.5194/amt-15-1811-
861 2022, 2022a.

862 Li, H., Riva, M., Rantala, P., Heikkinen, L., Daellenbach, K., Krechmer, J. E.,
863 Flaud, P.-M., Worsnop, D., Kulmala, M., Villenave, E., Perraudin, E., Ehn, M.,
864 and Bianchi, F.: Terpenes and their oxidation products in the French Landes
865 forest: insights from Vocus PTR-TOF measurements, *Atmos. Chem. Phys.*, 20,
866 1941-1959, 10.5194/acp-20-1941-2020, 2020.

867 Li, H., Canagaratna, M. R., Riva, M., Rantala, P., Zhang, Y., Thomas, S.,
868 Heikkinen, L., Flaud, P.-M., Villenave, E., Perraudin, E., Worsnop, D., Kulmala,
869 M., Ehn, M., and Bianchi, F.: Atmospheric organic vapors in two European pine
870 forests measured by a Vocus PTR-TOF: insights into monoterpene and
871 sesquiterpene oxidation processes, *Atmos. Chem. Phys.*, 21, 4123-4147,
872 10.5194/acp-21-4123-2021, 2021.

873 Li, K., Li, J., Tong, S., Wang, W., Huang, R.-J., and Ge, M.: Characteristics of
874 wintertime VOCs in suburban and urban Beijing: concentrations, emission
875 ratios, and festival effects, *Atmos. Chem. Phys.*, 19, 8021-8036, 10.5194/acp-
876 19-8021-2019, 2019.

877 Li, K., Zhang, J., Bell, D. M., Wang, T., Lamkaddam, H., Cui, T., Qi, L., Surdu,
878 M., Wang, D., Du, L., El Haddad, I., Slowik, J. G., and Prevot, A. S. H.:
879 Uncovering the dominant contribution of intermediate volatility compounds in
880 secondary organic aerosol formation from biomass-burning emissions, *Natl Sci*
881 *Rev*, 11, nwae014, 10.1093/nsr/nwae014, 2024a.

882 Li, X., Chen, Y., Li, Y., Cai, R., Li, Y., Deng, C., Wu, J., Yan, C., Cheng, H., Liu,
883 Y., Kulmala, M., Hao, J., Smith, J. N., and Jiang, J.: Seasonal variations in
884 composition and sources of atmospheric ultrafine particles in urban Beijing
885 based on near-continuous measurements, *Atmos. Chem. Phys.*, 23, 14801-
886 14812, 10.5194/acp-23-14801-2023, 2023.

887 Li, X.-B., Yuan, B., Wang, S., Wang, C., Lan, J., Liu, Z., Song, Y., He, X.,
888 Huangfu, Y., Pei, C., Cheng, P., Yang, S., Qi, J., Wu, C., Huang, S., You, Y.,
889 Chang, M., Zheng, H., Yang, W., Wang, X., and Shao, M.: Variations and
890 sources of volatile organic compounds (VOCs) in urban region: insights from
891 measurements on a tall tower, *Atmos. Chem. Phys.*, 22, 10567-10587,
892 10.5194/acp-22-10567-2022, 2022b.

893 Li, Y., Cai, R., Yin, R., Li, X., Yuan, Y., An, Z., Guo, J., Stolzenburg, D., Kulmala,
894 M., and Jiang, J.: A kinetic partitioning method for simulating the condensation
895 mass flux of organic vapors in a wide volatility range, *J. Aerosol Sci.*, 180,
896 10.1016/j.jaerosci.2024.106400, 2024b.

897 Liu, Q., Sheng, J., Wu, Y., Ma, Z., Sun, J., Tian, P., Zhao, D., Li, X., Hu, K., Li,
898 S., Shen, X., Zhang, Y., He, H., Huang, M., Ding, D., and Liu, D.: Source
899 characterization of volatile organic compounds in urban Beijing and its links to
900 secondary organic aerosol formation, *Sci. Total Environ.*,
901 10.1016/j.scitotenv.2022.160469, 2022.

902 Liu, Y., Yin, S., Zhang, S., Ma, W., Zhang, X., Qiu, P., Li, C., Wang, G., Hou, D.,
903 Zhang, X., An, J., Sun, Y., Li, J., Zhang, Z., Chen, J., Tian, H., Liu, X., and Liu,
904 L.: Drivers and impacts of decreasing concentrations of atmospheric volatile
905 organic compounds (VOCs) in Beijing during 2016-2020, *Sci Total Environ*, 906,
906 167847, 10.1016/j.scitotenv.2023.167847, 2023.

907 Millet, D. B., Baasandorj, M., Farmer, D. K., Thornton, J. A., Baumann, K.,
908 Brophy, P., Chaliyakunnel, S., de Gouw, J. A., Graus, M., Hu, L., Koss, A., Lee,
909 B. H., Lopez-Hilfiker, F. D., Neuman, J. A., Paulot, F., Peischl, J., Pollack, I. B.,
910 Ryerson, T. B., Warneke, C., Williams, B. J., and Xu, J.: A large and ubiquitous
911 source of atmospheric formic acid, *Atmos. Chem. Phys.*, 15, 6283-6304,
912 10.5194/acp-15-6283-2015, 2015.

913 Nie, W., Yan, C., Huang, D. D., Wang, Z., Liu, Y., Qiao, X., Guo, Y., Tian, L.,
914 Zheng, P., Xu, Z., Li, Y., Xu, Z., Qi, X., Sun, P., Wang, J., Zheng, F., Li, X., Yin,
915 R., Dallenbach, K. R., Bianchi, F., Petäjä, T., Zhang, Y., Wang, M., Schervish,
916 M., Wang, S., Qiao, L., Wang, Q., Zhou, M., Wang, H., Yu, C., Yao, D., Guo, H.,
917 Ye, P., Lee, S., Li, Y. J., Liu, Y., Chi, X., Kerminen, V.-M., Ehn, M., Donahue, N.
918 M., Wang, T., Huang, C., Kulmala, M., Worsnop, D., Jiang, J., and Ding, A.:
919 Secondary organic aerosol formed by condensing anthropogenic vapours over
920 China's megacities, *Nature Geoscience*, 15, 255-261, 10.1038/s41561-022-
921 00922-5, 2022.

922 Noziere, B., Kalberer, M., Claeys, M., Allan, J., D'Anna, B., Decesari, S., Finessi,
923 E., Glasius, M., Grgic, I., Hamilton, J. F., Hoffmann, T., Iinuma, Y., Jaoui, M.,
924 Kahnt, A., Kampf, C. J., Kourtev, I., Maenhaut, W., Marsden, N., Saarikoski,
925 S., Schnelle-Kreis, J., Surratt, J. D., Szidat, S., Szmigielski, R., and Wisthaler,
926 A.: The molecular identification of organic compounds in the atmosphere: state
927 of the art and challenges, *Chemical Reviews*, 115, 3919-3983,
928 10.1021/cr5003485, 2015.

929 Pan, S. and Wang, L.: Atmospheric oxidation mechanism of m-xylene initiated
930 by OH radical, *J Phys Chem A*, 118, 10778-10787, 10.1021/jp506815v, 2014.

931 Pfannerstill, E. Y., Arata, C., Zhu, Q., Schulze, B. C., Woods, R., Seinfeld, J. H.,
932 Bucholtz, A., Cohen, R. C., and Goldstein, A. H.: Volatile organic compound
933 fluxes in the agricultural San Joaquin Valley – spatial distribution, source
934 attribution, and inventory comparison, *Atmos. Chem. Phys.*, 23, 12753-12780,
935 10.5194/acp-23-12753-2023, 2023a.

936 Pfannerstill, E. Y., Arata, C., Zhu, Q., Schulze, B. C., Ward, R., Woods, R.,
937 Harkins, C., Schwantes, R. H., Seinfeld, J. H., Bucholtz, A., Cohen, R. C., and
938 Goldstein, A. H.: Temperature-dependent emissions dominate aerosol and
939 ozone formation in Los Angeles, *Science*, 384, 1324-1329,
940 doi:10.1126/science.adg8204, 2024.

941 Pfannerstill, E. Y., Arata, C., Zhu, Q., Schulze, B. C., Woods, R., Harkins, C.,
942 Schwantes, R. H., McDonald, B. C., Seinfeld, J. H., Bucholtz, A., Cohen, R. C.,
943 and Goldstein, A. H.: Comparison between Spatially Resolved Airborne Flux
944 Measurements and Emission Inventories of Volatile Organic Compounds in Los
945 Angeles, *Environ Sci Technol*, 57, 15533-15545, 10.1021/acs.est.3c03162,
946 2023b.

947 Pospisilova, V., Lopez-Hilfiker, F. D., Bell, D. M., El Haddad, I., Mohr, C., Huang,
948 W., Heikkinen, L., Xiao, M., Dommen, J., Prevot, A. S. H., Baltensperger, U.,
949 and Slowik, J. G.: On the fate of oxygenated organic molecules in atmospheric
950 aerosol particles, *Science Advances*, 6, eaax8922, doi:10.1126/sciadv.aax8922,
951 2020.

952 Priestley, M., Bannan, T. J., Le Breton, M., Worrall, S. D., Kang, S., Pullinen, I.,
953 Schmitt, S., Tillmann, R., Kleist, E., Zhao, D., Wildt, J., Garmash, O., Mehra, A.,
954 Bacak, A., Shallcross, D. E., Kiendler-Scharr, A., Hallquist, Å. M., Ehn, M., Coe,
955 H., Percival, C. J., Hallquist, M., Mentel, T. F., and McFiggans, G.: Chemical
956 characterisation of benzene oxidation products under high- and low-NOx
957 conditions using chemical ionisation mass spectrometry, *Atmos. Chem. Phys.*,
958 21, 3473-3490, 10.5194/acp-21-3473-2021, 2021.

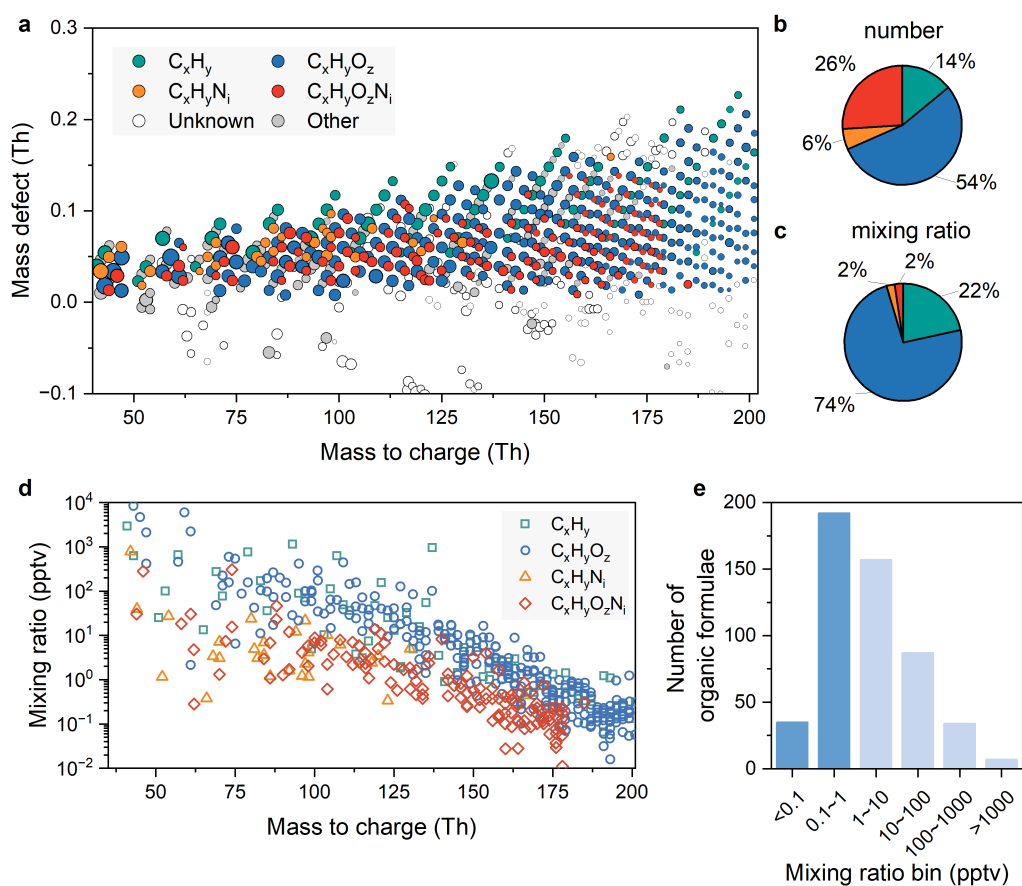
- 959 Pugliese, G., Ingrisch, J., Meredith, L. K., Pfannerstill, E. Y., Klupfel, T., Meeran,
960 K., Byron, J., Purser, G., Gil-Loaiza, J., van Haren, J., Dontsova, K.,
961 Kreuzwieser, J., Ladd, S. N., Werner, C., and Williams, J.: Effects of drought
962 and recovery on soil volatile organic compound fluxes in an experimental
963 rainforest, *Nat Commun*, 14, 5064, 10.1038/s41467-023-40661-8, 2023.
- 964 Qian, X., Shen, H., and Chen, Z.: Characterizing summer and winter carbonyl
965 compounds in Beijing atmosphere, *Atmos. Environ.*, 214,
966 10.1016/j.atmosenv.2019.116845, 2019.
- 967 Qiao, X., Zhang, Q., Wang, D., Hao, J., and Jiang, J.: Improving data reliability:
968 A quality control practice for low-cost PM(2.5) sensor network, *Sci Total Environ*,
969 779, 146381, 10.1016/j.scitotenv.2021.146381, 2021.
- 970 Reinecke, T., Leiminger, M., Jordan, A., Wisthaler, A., and Muller, M.: Ultrahigh
971 Sensitivity PTR-MS Instrument with a Well-Defined Ion Chemistry, *Anal Chem*,
972 95, 11879-11884, 10.1021/acs.analchem.3c02669, 2023.
- 973 Riva, M., Rantala, P., Krechmer, J. E., Peräkylä, O., Zhang, Y., Heikkinen, L.,
974 Garmash, O., Yan, C., Kulmala, M., Worsnop, D., and Ehn, M.: Evaluating the
975 performance of five different chemical ionization techniques for detecting
976 gaseous oxygenated organic species, *Atmos. Meas. Tech.*, 12, 2403-2421,
977 10.5194/amt-12-2403-2019, 2019.
- 978 Rolletter, M., Kaminski, M., Acir, I.-H., Bohn, B., Dorn, H.-P., Li, X., Lutz, A.,
979 Nehr, S., Rohrer, F., Tillmann, R., Wegener, R., Hofzumahaus, A., Kiendler-
980 Scharr, A., Wahner, A., and Fuchs, H.: Investigation of the α -pinene
981 photooxidation by OH in the atmospheric simulation chamber SAPHIR, *Atmos.*
982 *Chem. Phys.*, 19, 11635-11649, 10.5194/acp-19-11635-2019, 2019.
- 983 Sekimoto, K., Li, S.-M., Yuan, B., Koss, A., Coggon, M., Warneke, C., and de
984 Gouw, J.: Calculation of the sensitivity of proton-transfer-reaction mass
985 spectrometry (PTR-MS) for organic trace gases using molecular properties, *Int.*
986 *J. Mass Spectrom.*, 421, 71-94, 10.1016/j.ijms.2017.04.006, 2017.
- 987 Sheng, J., Zhao, D., Ding, D., Li, X., Huang, M., Gao, Y., Quan, J., and Zhang,
988 Q.: Characterizing the level, photochemical reactivity, emission, and source
989 contribution of the volatile organic compounds based on PTR-TOF-MS during
990 winter haze period in Beijing, China, *Atmospheric Research*, 212, 54-63,
991 10.1016/j.atmosres.2018.05.005, 2018.
- 992 Sreeram, A., Blomdahl, D., Misztal, P., and Bhasin, A.: High resolution chemical
993 fingerprinting and real-time oxidation dynamics of asphalt binders using Vocus
994 Proton Transfer Reaction (PTR-TOF) mass spectrometry, *Fuel*, 320,
995 10.1016/j.fuel.2022.123840, 2022.
- 996 Thomas, S. J., Li, H., Praplan, A. P., Hellén, H., and Bianchi, F.: Complexity of
997 downy birch emissions revealed by Vocus proton transfer reaction time-of-flight
998 mass spectrometer, *Frontiers in Forests and Global Change*, 5,
999 10.3389/ffgc.2022.1030348, 2022.
- 1000 Vermeuel, M. P., Novak, G. A., Kilgour, D. B., Clafin, M. S., Lerner, B. M.,
1001 Trowbridge, A. M., Thom, J., Cleary, P. A., Desai, A. R., and Bertram, T. H.:
1002 Observations of biogenic volatile organic compounds over a mixed temperate
1003 forest during the summer to autumn transition, *Atmos. Chem. Phys.*, 23, 4123-
1004 4148, 10.5194/acp-23-4123-2023, 2023.
- 1005 Vettikkat, L., Miettinen, P., Buchholz, A., Rantala, P., Yu, H., Schallhart, S.,
1006 Petäjä, T., Seco, R., Männistö, E., Kulmala, M., Tuittila, E.-S., Guenther, A. B.,
1007 and Schobesberger, S.: High emission rates and strong temperature response
1008 make boreal wetlands a large source of isoprene and terpenes, *Atmos. Chem.*

- 1009 Phys., 23, 2683-2698, 10.5194/acp-23-2683-2023, 2023.
- 1010 Wang, L., Slowik, J. G., Tong, Y., Duan, J., Gu, Y., Rai, P., Qi, L., Stefenelli, G.,
1011 Baltensperger, U., Huang, R.-J., Cao, J., and Prévôt, A. S. H.: Characteristics
1012 of wintertime VOCs in urban Beijing: Composition and source apportionment,
1013 Atmospheric Environment: X, 9, 10.1016/j.aeaoa.2020.100100, 2021a.
- 1014 Wang, M., Chen, D., Xiao, M., Ye, Q., Stolzenburg, D., Hofbauer, V., Ye, P.,
1015 Vogel, A. L., Mauldin, R. L., 3rd, Amorim, A., Baccarini, A., Baumgartner, B.,
1016 Brilke, S., Dada, L., Dias, A., Duplissy, J., Finkenzeller, H., Garmash, O., He, X.
1017 C., Hoyle, C. R., Kim, C., Kvashnin, A., Lehtipalo, K., Fischer, L., Molteni, U.,
1018 Petaja, T., Pospisilova, V., Quelever, L. L. J., Rissanen, M., Simon, M., Tauber,
1019 C., Tome, A., Wagner, A. C., Weitz, L., Volkamer, R., Winkler, P. M., Kirkby, J.,
1020 Worsnop, D. R., Kulmala, M., Baltensperger, U., Dommen, J., El-Haddad, I.,
1021 and Donahue, N. M.: Photo-oxidation of Aromatic Hydrocarbons Produces Low-
1022 Volatility Organic Compounds, Environ Sci Technol, 54, 7911-7921,
1023 10.1021/acs.est.0c02100, 2020a.
- 1024 Wang, W., Yuan, B., Su, H., Cheng, Y., Qi, J., Wang, S., Song, W., Wang, X.,
1025 Xue, C., Ma, C., Bao, F., Wang, H., Lou, S., and Shao, M.: A large role of missing
1026 volatile organic compound reactivity from anthropogenic emissions in ozone
1027 pollution regulation, Atmos. Chem. Phys., 24, 4017-4027, 10.5194/acp-24-
1028 4017-2024, 2024.
- 1029 Wang, Y., Yang, G., Lu, Y., Liu, Y., Chen, J., and Wang, L.: Detection of gaseous
1030 dimethylamine using vocus proton-transfer-reaction time-of-flight mass
1031 spectrometry, Atmos. Environ., 243, 10.1016/j.atmosenv.2020.117875, 2020b.
- 1032 Wang, Y., Mehra, A., Krechmer, J. E., Yang, G., Hu, X., Lu, Y., Lambe, A.,
1033 Canagaratna, M., Chen, J., Worsnop, D., Coe, H., and Wang, L.: Oxygenated
1034 products formed from OH-initiated reactions of trimethylbenzene: autoxidation
1035 and accretion, Atmos. Chem. Phys., 20, 9563-9579, 10.5194/acp-20-9563-
1036 2020, 2020c.
- 1037 Wang, Z., Ehn, M., Rissanen, M. P., Garmash, O., Quelever, L., Xing, L.,
1038 Monge-Palacios, M., Rantala, P., Donahue, N. M., Berndt, T., and Sarathy, S.
1039 M.: Efficient alkane oxidation under combustion engine and atmospheric
1040 conditions, Commun Chem, 4, 18, 10.1038/s42004-020-00445-3, 2021b.
- 1041 Wennberg, P. O., Bates, K. H., Crouse, J. D., Dodson, L. G., McVay, R. C.,
1042 Mertens, L. A., Nguyen, T. B., Praske, E., Schwantes, R. H., Smarte, M. D., St
1043 Clair, J. M., Teng, A. P., Zhang, X., and Seinfeld, J. H.: Gas-Phase Reactions of
1044 Isoprene and Its Major Oxidation Products, Chem. Rev., 118, 3337-3390,
1045 10.1021/acs.chemrev.7b00439, 2018.
- 1046 Williams, J. and Koppmann, R.: Volatile Organic Compounds in the Atmosphere:
1047 An Overview, in: Volatile Organic Compounds in the Atmosphere, 1-32,
1048 <https://doi.org/10.1002/9780470988657.ch1>, 2007.
- 1049 Wohl, C., Güell-Bujons, Q., Castillo, Y. M., Calbet, A., and Simó, R.: Volatile
1050 Organic Compounds Released by *Oxyrrhis marina* Grazing on *Isochrysis*
1051 *galbana*, Oceans, 4, 151-169, 10.3390/oceans4020011, 2023.
- 1052 Wu, C., Wang, C., Wang, S., Wang, W., Yuan, B., Qi, J., Wang, B., Wang, H.,
1053 Wang, C., Song, W., Wang, X., Hu, W., Lou, S., Ye, C., Peng, Y., Wang, Z.,
1054 Huangfu, Y., Xie, Y., Zhu, M., Zheng, J., Wang, X., Jiang, B., Zhang, Z., and
1055 Shao, M.: Measurement report: Important contributions of oxygenated
1056 compounds to emissions and chemistry of volatile organic compounds in urban
1057 air, Atmos. Chem. Phys., 20, 14769-14785, 10.5194/acp-20-14769-2020, 2020.
- 1058 Xu, X., Stee, L. L. P., Williams, J., Beens, J., Adahchour, M., Vreuls, R. J. J.,

- 1059 Brinkman, U. A., and Lelieveld, J.: Comprehensive two-dimensional gas
1060 chromatography (GC × GC) measurements of volatile organic compounds in
1061 the atmosphere, *Atmospheric Chemistry & Physics*, 3, 665-682, 2003.
- 1062 Yacovitch, T. I., Lerner, B. M., Canagaratna, M. R., Daube, C., Healy, R. M.,
1063 Wang, J. M., Fortner, E. C., Majluf, F., Claflin, M. S., Roscioli, J. R., Lunny, E.
1064 M., and Herndon, S. C.: Mobile Laboratory Investigations of Industrial Point
1065 Source Emissions during the MOOSE Field Campaign, *Atmosphere*, 14,
1066 10.3390/atmos14111632, 2023.
- 1067 Yang, X., Wang, H., Lu, K., Ma, X., Tan, Z., Long, B., Chen, X., Li, C., Zhai, T.,
1068 Li, Y., Qu, K., Xia, Y., Zhang, Y., Li, X., Chen, S., Dong, H., Zeng, L., and Zhang,
1069 Y.: Reactive aldehyde chemistry explains the missing source of hydroxyl
1070 radicals, *Nat Commun*, 15, 1648, 10.1038/s41467-024-45885-w, 2024.
- 1071 Ye, C., Yuan, B., Lin, Y., Wang, Z., Hu, W., Li, T., Chen, W., Wu, C., Wang, C.,
1072 Huang, S., Qi, J., Wang, B., Wang, C., Song, W., Wang, X., Zheng, E.,
1073 Krechmer, J. E., Ye, P., Zhang, Z., Wang, X., Worsnop, D. R., and Shao, M.:
1074 Chemical characterization of oxygenated organic compounds in the gas phase
1075 and particle phase using iodide CIMS with FIGAERO in urban air, *Atmos. Chem.*
1076 *Phys.*, 21, 8455-8478, 10.5194/acp-21-8455-2021, 2021.
- 1077 Yu, Y., Guo, S., Wang, H., Shen, R., Zhu, W., Tan, R., Song, K., Zhang, Z., Li,
1078 S., Chen, Y., and Hu, M.: Importance of Semivolatile/Intermediate-Volatility
1079 Organic Compounds to Secondary Organic Aerosol Formation from Chinese
1080 Domestic Cooking Emissions, *Environ. Sci. Technol.*,
1081 10.1021/acs.estlett.2c00207, 2022.
- 1082 Yuan, B., Koss, A. R., Warneke, C., Coggon, M., Sekimoto, K., and de Gouw,
1083 J. A.: Proton-Transfer-Reaction Mass Spectrometry: Applications in
1084 Atmospheric Sciences, *Chem. Rev.*, 117, 13187-13229,
1085 10.1021/acs.chemrev.7b00325, 2017.
- 1086 Yuan, B., Koss, A., Warneke, C., Gilman, J. B., Lerner, B. M., Stark, H., and de
1087 Gouw, J. A.: A high-resolution time-of-flight chemical ionization mass
1088 spectrometer utilizing hydronium ions (H₃O⁺ ToF-CIMS) for measurements of
1089 volatile organic compounds in the atmosphere, *Atmos. Meas. Tech.*, 9, 2735-
1090 2752, 10.5194/amt-9-2735-2016, 2016.
- 1091 Yuan, Q., Zhang, Z., Chen, Y., Hui, L., Wang, M., Xia, M., Zou, Z., Wei, W., Ho,
1092 K. F., Wang, Z., Lai, S., Zhang, Y., Wang, T., and Lee, S.: Origin and
1093 transformation of volatile organic compounds at a regional background site in
1094 Hong Kong: Varied photochemical processes from different source regions, *Sci*
1095 *Total Environ*, 168316, 10.1016/j.scitotenv.2023.168316, 2023.
- 1096 Zaytsev, A., Breitenlechner, M., Koss, A. R., Lim, C. Y., Rowe, J. C., Kroll, J. H.,
1097 and Keutsch, F. N.: Using collision-induced dissociation to constrain sensitivity
1098 of ammonia chemical ionization mass spectrometry (NH₄⁺ CIMS) to
1099 oxygenated volatile organic compounds, *Atmos Meas Tech*, 12, 1861-1870,
1100 10.5194/amt-12-1861-2019, 2019a.
- 1101 Zaytsev, A., Koss, A. R., Breitenlechner, M., Krechmer, J. E., Nihill, K. J., Lim,
1102 C. Y., Rowe, J. C., Cox, J. L., Moss, J., Roscioli, J. R., Canagaratna, M. R.,
1103 Worsnop, D. R., Kroll, J. H., and Keutsch, F. N.: Mechanistic study of the
1104 formation of ring-retaining and ring-opening products from the oxidation of
1105 aromatic compounds under urban atmospheric conditions, *Atmos Chem Phys*,
1106 19, 15117-15129, 10.5194/acp-19-15117-2019, 2019b.
- 1107 Zhang, Y., Xu, W., Zhou, W., Li, Y., Zhang, Z., Du, A., Qiao, H., Kuang, Y., Liu,
1108 L., Zhang, Z., He, X., Cheng, X., Pan, X., Fu, Q., Wang, Z., Ye, P., Worsnop, D.
1109 R., and Sun, Y.: Characterization of organic vapors by a Vocus proton-transfer-

- 1110 reaction mass spectrometry at a mountain site in southeastern China, *Sci Total*
1111 *Environ*, 919, 170633, 10.1016/j.scitotenv.2024.170633, 2024.
- 1112 Zhao, J. and Zhang, R.: Proton transfer reaction rate constants between
1113 hydronium ion (H₃O⁺) and volatile organic compounds, *Atmos. Environ.*, 38,
1114 2177-2185, 10.1016/j.atmosenv.2004.01.019, 2004.
- 1115
1116

1117 **Figures**

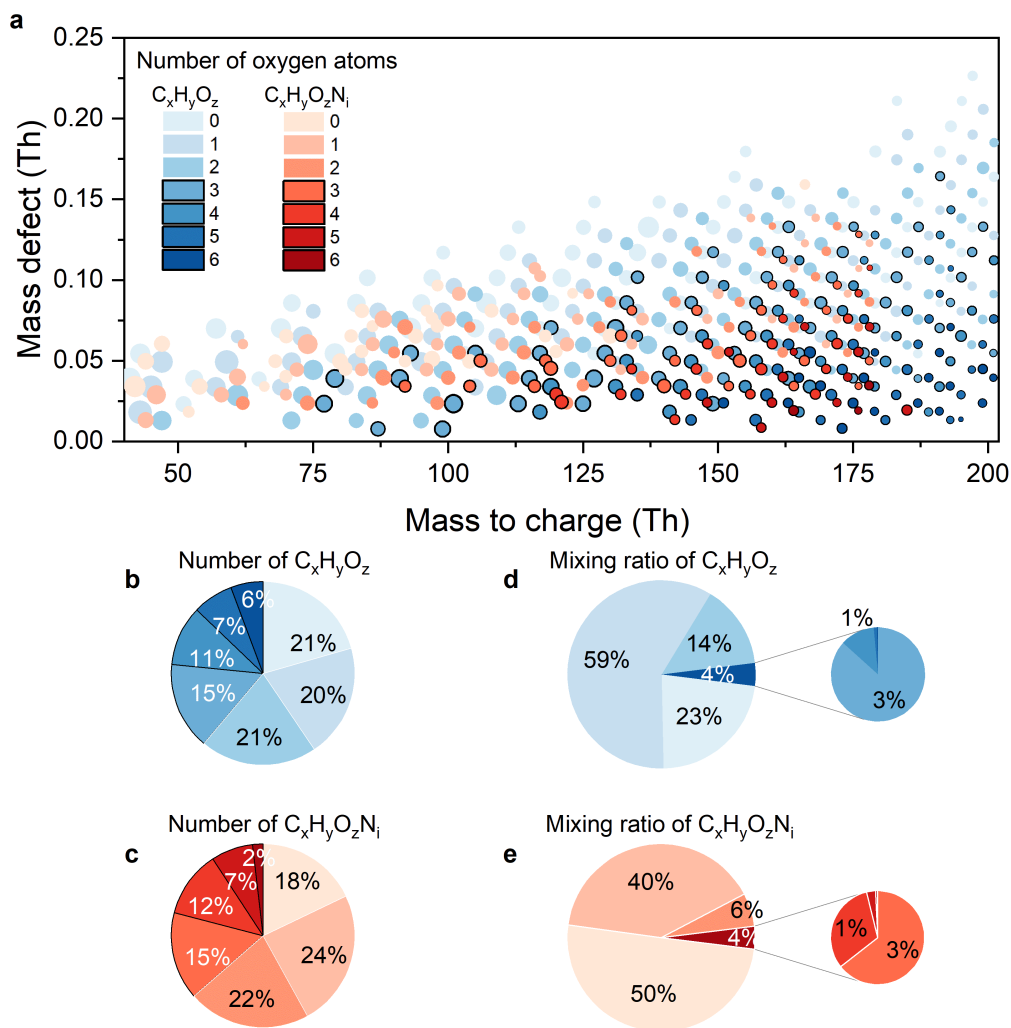


1118

1119 Figure 1. Identified formulae in urban Beijing using Vocus-PTR. (a) Mass defect
 1120 plot. The sizes of the bubbles represent the annual median mixing ratios. The
 1121 bubbles are colored by different elemental compositions as labeled in the
 1122 legend. The “unknown” refers to fitted peaks without matched formula. The
 1123 “other” refers to peaks containing elements other than C, H, O, and N or
 1124 fragment peaks (or radicals). (b) Pie chart of the number of identified formulae.
 1125 (c) Pie chart of the annual median mixing ratios of identified formulae. The color
 1126 scheme of the pie charts is the same to that of the mass defect plot. (d) The
 1127 annual median mixing ratios of identified formulae versus their masses. (e)
 1128 Histogram of annual mixing ratios of identified formulae. Bins with values less
 1129 than 1 ppt are emphasized in dark blue color.

1130

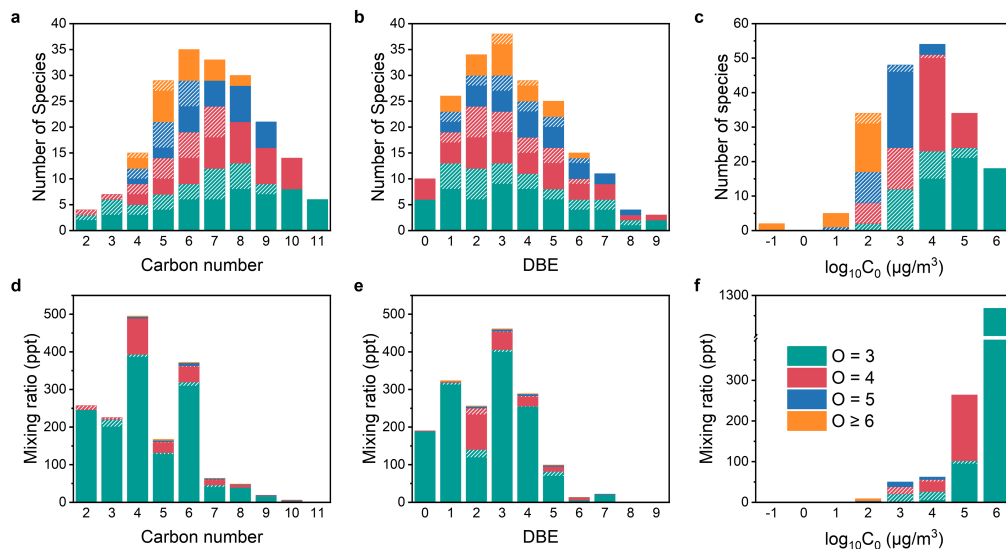
1131



1132

1133 Figure 2. Organic vapors of different oxygen content. (a) Mass defect plot. The
 1134 sizes of the bubbles represent the annual median mixing ratios. The bubbles
 1135 are colored by different oxygen numbers as labeled in the legend. Bubbles
 1136 representing organic vapors with 3 or more oxygens are highlighted with black
 1137 borders. Bars labeled as 6 refers to organic vapors with oxygen number equal
 1138 or larger than 6. (b) Pie chart of the number of $C_xH_yO_z$ species. (c) Pie chart of
 1139 the number of $C_xH_yO_zN_i$ species. (d) Pie chart of the mixing ratio of $C_xH_yO_z$
 1140 species. (e) Pie chart of the mixing ratio of $C_xH_yO_zN_i$ species. The color scheme
 1141 of the pie charts is the same to that of the mass defect plot.

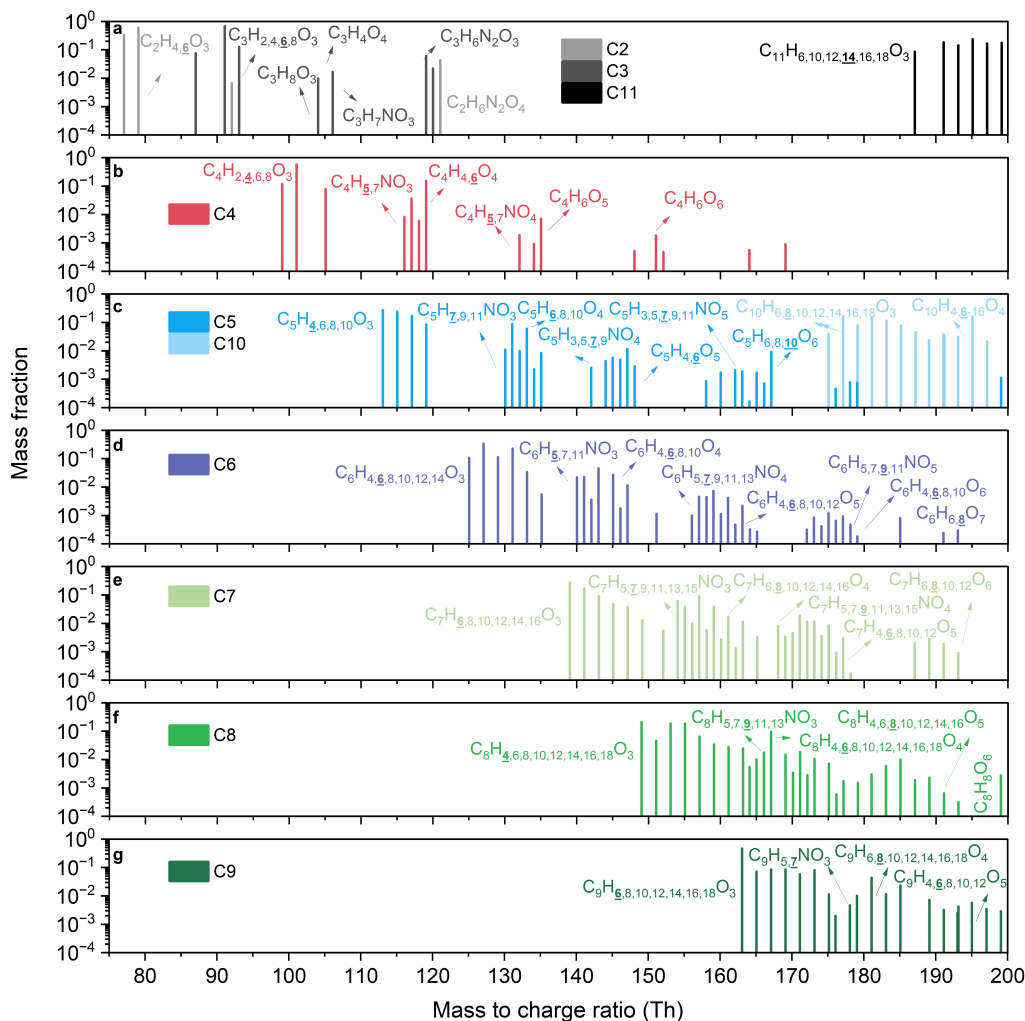
1142



1143

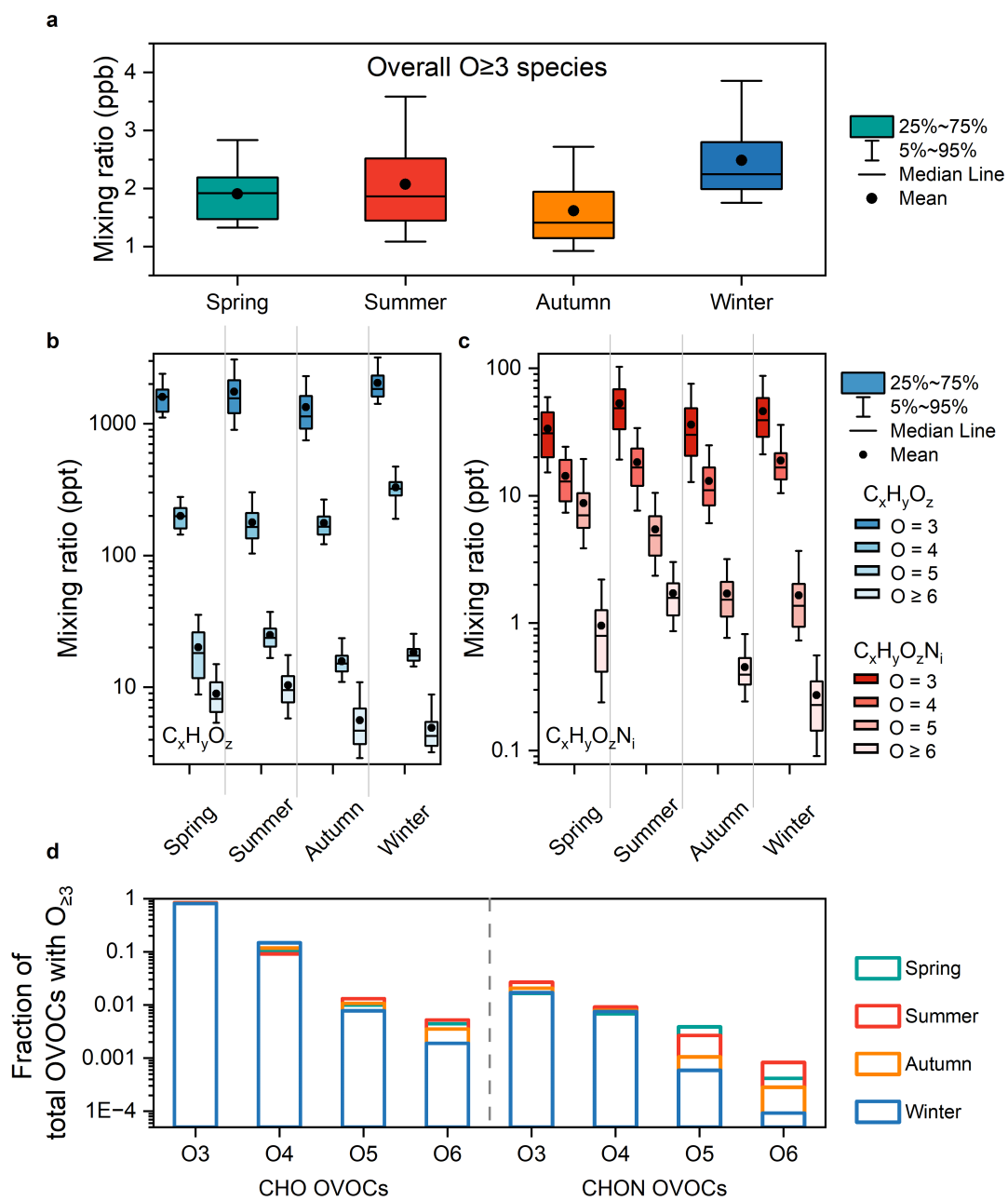
1144 Figure 3. Distribution of carbon number, double bond equivalent (DBE), and
 1145 volatility of organic vapors with multiple oxygens. Panels (a) - (c) represent
 1146 species number distributions of carbon number, DBE, and volatility, respectively.
 1147 Panels (d) - (e) represent mixing ratio distributions of carbon number, DBE, and
 1148 volatility, respectively. Different color of bars refers to compounds with different
 1149 oxygen content. Bars without white stripes represent $C_xH_yO_{\geq 3}$, while shaded
 1150 bars with white stripes represent $C_xH_yO_{\geq 3}N$. Y axes refer to annual median
 1151 mixing ratios.

1152



1153

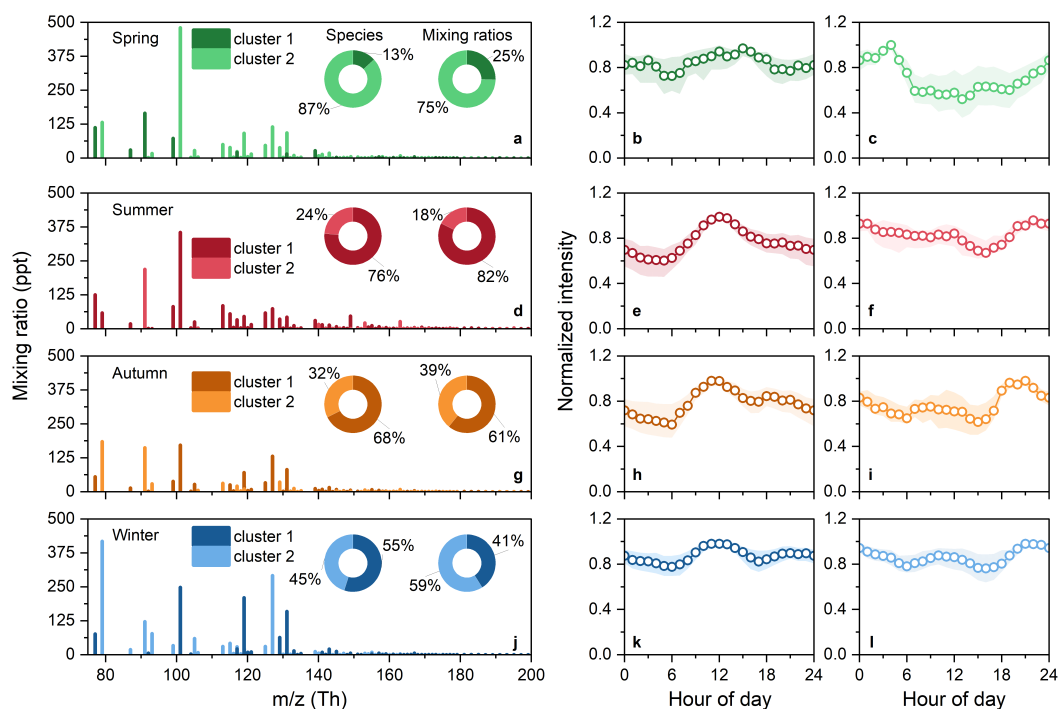
1154 Figure 4. Mass spectra of organic vapors with multiple oxygens with different
 1155 carbon numbers: (a) C2, C3, and C11; (b) C4; (c) C5 and C10; (d) C6; (e) C7;
 1156 (f) C8; (g) C9. The y axis shows the annual median mixing ratio fraction of
 1157 organic vapors for each carbon number, which means that for different organic
 1158 vapors with the same carbon number, the sum of the mixing ratio fractions
 1159 equals 1. The unprotonated formulae of organics vapors with multiple oxygens
 1160 are labelled. In molecular formulas with the same number of carbons and
 1161 oxygens, the hydrogen content in the organic vapors with the highest intensity
 1162 is emphasized by bold and underlined formatting.



1163

1164 Figure 5. Seasonal variations of organic vapors with multiple oxygens in urban
 1165 Beijing. (a) Total organic vapors with multiple oxygens. (b) C_xH_yO_z with different
 1166 oxygens. (c) C_xH_yO_zN_i with different oxygens. (d) Fractions of organic vapors
 1167 with different oxygens of total organic vapors with multiple oxygens.

1168



1169

1170 Figure 6. Cluster results of organic vapors with multiple oxygens in four seasons.
 1171 (a) – (c) Cluster results for spring. (a) Mass spectra of organic vapors with
 1172 multiple oxygens in spring. Y axis is the median mixing ratio of each compound.
 1173 Two different shades of colors are used to distinguish between two clusters.
 1174 Two pie charts represent the distribution of species numbers and mixing ratios
 1175 of organic vapors for two clusters. (b) Normalized median diurnal variation of
 1176 cluster 1, daytime cluster. (c) Normalized median diurnal variation of cluster 2,
 1177 nighttime cluster. The shaded areas in the graph (b) and (c) represent the 25th
 1178 and 75th percentiles. (d) – (f) Cluster results for summer. (g) to (i) Cluster results
 1179 for autumn. (j) – (l) Cluster results for winter.